Design of an Energy Storing Orthosis for Providing Gait to People with Spinal Cord Injury

A Thesis
SUBMITTED TO THE FACULTY OF
UNIVERSITY OF MINNESOTA
BY

Kyle J. Boughner

IN PARTIAL FULFILLMENT OF THE REQUIREMENTS
FOR THE DEGREE OF
MASTER OF SCIENCE IN MECHANICAL ENGINEERING

William K. Durfee, Advisor

May 2014

Abstract

A new design is proposed for an energy storing orthosis (ESO) that restores walking to people with spinal cord injury by combining functional electrical stimulation of the quadriceps muscle with a mechanical brace that uses elastic elements to store and transfer energy between hip and knee joints. The new ESO is a variation of a previous design and uses constant force springs for energy storage. A study was completed investigating gait dynamics of the ESO. Preliminary assessment, using simulations and prototype testing indicates that the design has demonstrated technical feasibility and that constant force springs are a viable option for accomplishing gait in the ESO.

Table of Contents

List of Tables

List of Figures

Chapter 1. Introduction

1.1 Overview

Individuals with spinal cord injury (SCI) have limited modes of transportation. The wheelchair is the most common mobility aid, but 64% of SCI respondents prioritized walking as the main form of mobility to experience again [1]. Standing is another priority at 25%, and can provide health benefits compared to spending long periods in a wheelchair [2]. There are 273,000 people living with SCI injuries in the U.S. with approximately 12,000 new cases each year [3].

Several technologies that enable people with paraplegic SCI to stand or walk have been developed [4]. They include functional electrical stimulation (FES), externally powered orthosis, and orthotic bracing. FES is the contraction of muscles by electrical stimulation to cause or drive limb movement. This technology has been shown to improve health and longevity of the user and their muscles [2], [5]–[10]. Electrodes that cause stimulation are connected to the muscles by implantation directly into the muscle or on the surface of the skin. Implantation is done through surgical techniques and is usually left in the muscle permanently [11], [12]. By stimulating multiple muscles systematically FES can produce assisted standing and gait [8], [12]–[15]. There are limitations when using FES alone to achieve gait. Muscle fatigue can occur quickly when using FES [16]. Depending on which muscles are being stimulated, placement of the electrodes can be difficult to

achieve optimal muscle output for both implanted and surface stimulation. Joint control can also be difficult using FES because of the high number of degrees of freedom and because muscle output is not repeatable with stimulation input.

Externally powered exoskeletons generate torque to drive the joints to achieve gait [17]–[19]. Figure 1.1 is an example of a powered exoskeleton from Farris et al. The power sources vary and examples include batteries and pneumatics. Electric motors are the most common way to drive the joint with rigid orthotic bracing on each leg. Since external power is needed, power sources must be incorporated into the device, which can lead to the device being heavy and the user carrying large loads usually in the head-arm-torso (HAT) region. Also, external power sources can quickly run out of energy, which makes these devices impractical for everyday use.

Figure 1.1 - Externally powered exoskeleton, reprinted from [18]

Hybrid devices combine useful aspects of the different gait technologies [20]–[29]. One type of hybrid device combines FES with orthotic bracing for better joint control. Using this concept, muscle fatigue can be reduced by better joint control and by locking the joints and relaxing the stimulated muscle to conserve energy as the walking cycle advances. For example, Goldfarb et al. used magnetic particle brakes for joint control with FES [22], [27] (Figure 1.2). Another concept for a hybrid device was developed by Quintero et al., who completed the preliminary design of the joint coupled orthosis (JCO) [25].

Figure 1.2 - Controlled brake orthosis, reprinted from [22]

1.2 Previous Art

The energy storing orthosis (ESO) is another type of hybrid device [21], [24], [26], [28] (Figure 1.3). The ESO stored energy and used the energy with specific timing to drive gait. The advantage of this device is that no external power source is needed other than the power for muscle stimulation. Further, with the ESO, stimulation of only one muscle can provide the energy that is stored in the device. This indicates that the ESO devices should be lighter than the externally powered gait devices.

Figure 1.3 - 2nd generation ESO, reprinted from [24]

The work by Rivard et al. was the initial design of the ESO device [21], [26]. Several energy storage elements were considered for the walking device including mechanical springs, gas springs, and pneumatic air cylinders. Gas springs were chosen as the ESO energy storage elements because of their stored energy to weight ratio compared to other components.

The second generation of the ESO device used a different energy storage element and addressed the design issue of locking the joints throughout gait [28]. Gas springs, from the previous ESO, were determined to be inadequate for the new design. Instead of the gas springs, elastomer bands were the new energy storage element explored. Rubber

bands were used instead of gas springs because of two characteristics: their ability to store energy in a package that is small and light, and their ability to stretch many times the original length. Also the various sizes of bands and the ability to quickly add or remove bands to the device made them a desirable design choice.

The next phase of the second generation ESO design optimized the energy storage elements [24]. No components or systems were changed from the previous design. Instead, the new design improved component force characteristics and mounting locations of the previous ESO. The goal of the study was to transfer energy as efficiently as possible from the quadriceps to the knee and hip while maintaining adequate posture and consistent joint range of motion. The system was simulated using Matlab, and accounted for force/torque, power and energy requirements of the energy storing systems. Results from the study were the number of rubber bands and mounting locations for the ESO energy storage systems. Previous art has shown that the ESO concept is feasible, but has flaws that limit performance. More information on the previous ESO art is in Appendix A.

Several issues limit the capabilities of the previous ESO devices. Upper body support was an issue with the ESO for providing both comfort and rigidity needed for reaching gait trajectories. Another issue was the user's inability to sit in a wheelchair. Periodic resting is needed for SCI users, making this design undesirable. Another issue was the long don

and doff time, and difficulty for the user to perform this task. A potential reason for this difficulty is the bracing on the inside of the legs requiring the device to be slid onto the leg from behind instead of on the side if only straps were present on the inside of the user's leg. Problems have been encountered with the energy storage bands not working as intended and wearing out quickly. The profile and packaging of the device's components was also a concern and future ESO versions should limit the main components to the thigh.

1.3 Objective

The new ESO design presented in this thesis is based on previous ESO work [21], [24], [26], [28], but uses constant force springs to store and transfer energy, rather than the pneumatic and elastomeric springs used previously. The new ESO uses FES of the quadriceps to extend the knee and also to provide energy to storage elements to produce the gait sequence in Figure 1.4. The quadriceps muscle is a suitable muscle for surface FES because of its large area and ease of electrode placement. Once the muscle energy is stored and the FES switched off, the hip and knee joints are locked and unlocked with specific timing to prevent muscle fatigue.

The purpose of the project was to determine if the new ESO concept is feasible to justify continuing development. Technical feasibility was assessed by a study of the hip and knee joint's static and dynamic properties during gait. The focus of this research is on the

hip and knee joint mechanisms, which are novel, and not on the entire orthosis or body attachment points, which are conventional. Figure 1.5 is a simplified ESO thigh segment concept with the hip and knee components.

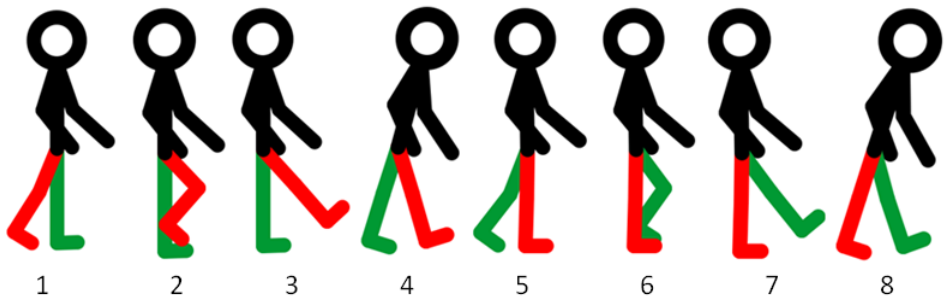

Figure 1.4 - ESO primitive gait cycle. The right leg actuation takes place during step 1-4 and left leg actuation takes place in steps 5-8.

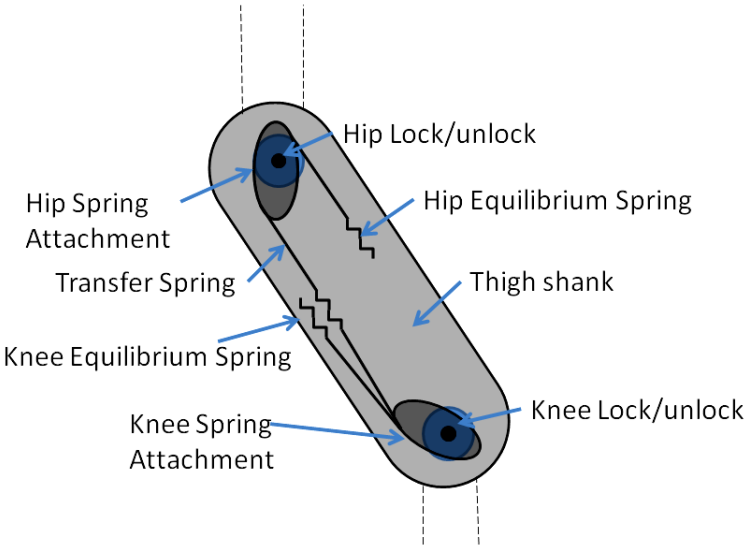

Figure 1.5 - ESO thigh segment that houses main ESO gait components

1.4 ESO Concept

Gait Cycle

The ESO walking motion models a primitive gait stepping sequence in Figure 1.4. Conventional gait is more complex involving ankle flexion and extension to provide forward propulsion. The forward progression of primitive gait is the falling forward of the foot, steps 4 and 8 in Figure 1.4, until it comes into contact with the ground.

The gait produced by the ESO has four phases (Figure 1.6): equilibrium, stimulation, foot ground contact, and hip extension.

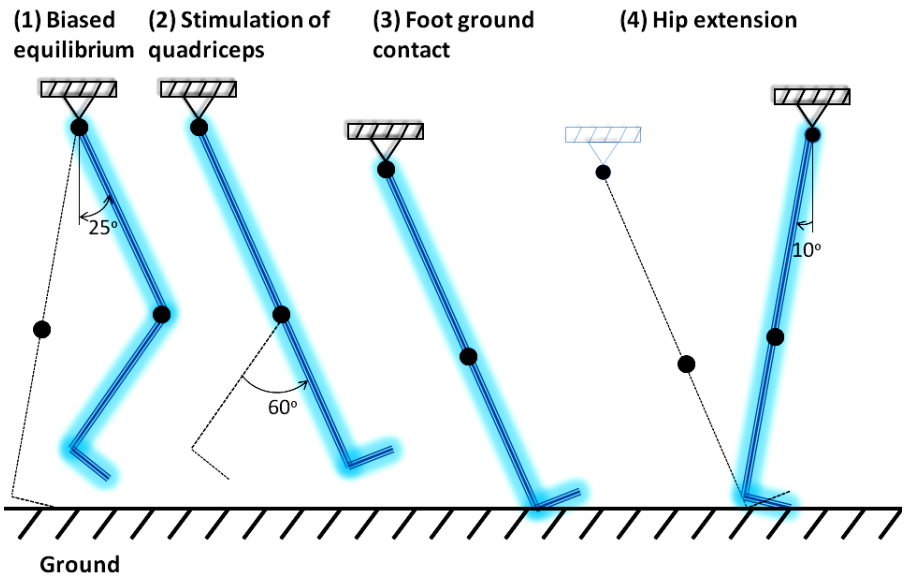

Figure 1.6 - Four phases of gait. (1) is the biased equilibrium position of the leg. (2) is the stimulation of the quadriceps causing knee extension and energy storage in the spring elements. (3) is the fall forward of the user to the ground. (4) is the hip extension energy release.

The first phase of the gait cycle is the biased equilibrium position of the leg. To hold the leg in place at this position a locking mechanism is needed at the hip and knee joints, or gravity would prevent the leg from staying at these angles. Springs at the hip and knee are used to move and hold the leg against gravity when the locking mechanism is unlocked.

To transition to the second phase, FES of the quadriceps is applied that results in the knee swinging to full extension (Figure 1.6). To prevent muscle fatigue the knee joint is locked at full extension and the FES switched off. During knee extension energy from the quadriceps is also delivered to a transfer spring that releases its energy at a later point in the gait cycle. After the knee is fully extended, the user falls forward onto the foot of this extended leg to the foot ground contact position.

The transition to the hip extension phase occurs through energy release from the transfer spring into the hip joint. The locking mechanism at the hip is important to conserve quadriceps energy from being released at improper times during gait. The final release of quadriceps energy takes place as the leg moves from phase 4 back to phase 1, when the springs around the hip and knee joints flex the leg back to the starting equilibrium position.

Joint Range of Motion

The required joint ranges of motion are taken from Goldfarb et al. [22]. During the gait cycle the hip joint actuates from 25 degrees of flexion to 10 degrees of extension. The range of motion of the knee joint is from full extension to 60 degrees of flexion. Joint rotation in the sagittal plane is used in the development of the gait cycle (Figure 1.7).

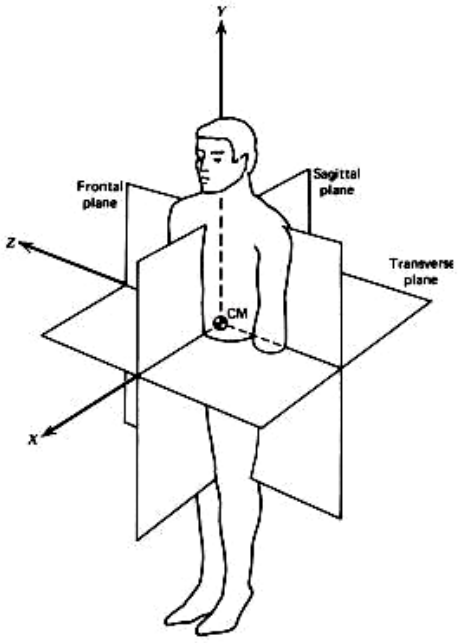

Figure 1.7 - Spatial body planes, reprinted from [30, p. 47]

This means that the hip and knee joints are modeled and act as pin joints. By restricting rotation of the joints to pin joints in the sagittal plane, the joint is simpler saving space and weight. Rotation in the transverse and frontal planes occurs during conventional gait, but will be mitigated by the orthotic bracing of the ESO system.

Available Quadriceps Torque

The available quadriceps torque must be defined to accomplish gait using FES. The quadriceps is used to drive the energy storing components in the ESO device. A previous study investigated the torque output of the quadriceps as a function of knee flexion [16]. For the ESO the knee is at 60 degrees of flexion when stimulated. This corresponds to the highest available torque output of the quadriceps muscle (Figure 1.8).

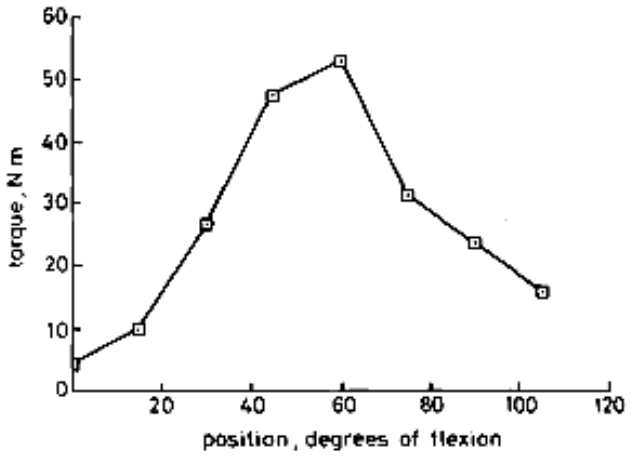

Figure 1.8 - Available quadriceps stimulation torque, reprinted from [16]

The torque available at this position is about 53 Nm. This means that the ESO cannot expect the quadriceps to deliver more than the 53 Nm of torque to drive gait.

Leg Kinematics

To begin detailing a design for the ESO device leg parameters must be defined. Parameters used were the average male's height and weight of 1.75 m and 79.5 kg [31].

The leg lengths, weights and center of gravity are the variables recorded for the ESO project. The thigh, shin and foot lengths can be determined by taking a fraction of the whole body height [30]. Appendix B is used for finding the weight and center of gravity of the segments.

Once the leg characteristics were defined, the needed joint torque can be found for the design based on the hip and knee joint's range of motion. A static analysis determines the torque at the hip and knee joints due to gravity. This torque found using static analysis represents the torque due to the leg's center of mass position during the joint range of motion. As the legs are flexed the center of mass of the leg segments is moved further away from the joints resulting in a larger torque on the joint. For both the hip and the knee joints the leg force from the center of mass was calculated from the leg kinematics. Then the center of mass distance from the joint was calculated over the joint range of motion. Figure 1.9 shows the static gravity torque seen at the hip and knee joints using the calculated leg center of mass information.

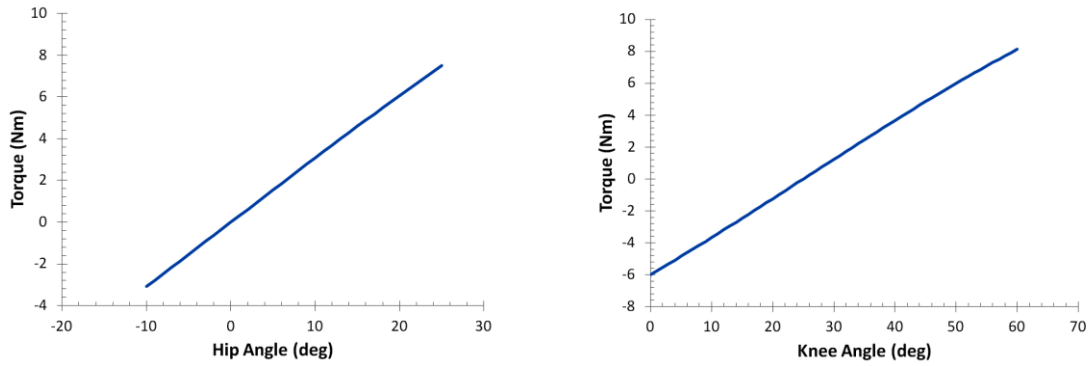

Figure 1.9 - Joint torques due to gravity for hip and knee joints

This information is needed when designing the ESO device because the energy storing components will have to supply more torque at the joints than the gravity torque, to hold the leg at the desired joint angles. If the components do not have enough torque at the joints, gravity will cause the leg to swing and not reach the desired angles.

ESO Components

Three energy storage and release elements are needed for the four phases of primitive gait. When the quadriceps is stimulated energy is stored in the transfer spring and the knee equilibrium spring. The transfer spring is used to drive hip extension and the knee equilibrium spring returns the knee joint back to the flexed equilibrium position. The third spring is the hip equilibrium spring which brings the hip joint back to the equilibrium position in the last phase of the gait cycle. Consideration for the type of springs used is the main design challenge, so that the available quadriceps torque is used

as efficiently as possible. An attachment point for the spring elements is needed that best matches the gravity torque profiles of the joints. Another component needed is the locking mechanism of the hip and knee joints. These components hold the joints at any angle in the joint's range of motion. Important considerations for the locking components will be size and profile, weight, actuation and performance. Later sections will detail the considerations and choices of the main elements for completing the ESO concept.

1.5 Design Requirements

Table 1.1 shows the design specifications for the ESO. Requirements 1 and 2 enable the user to sit in a wheelchair with the device. This is needed when resting, and also for donning and doffing the device. Requirement 3 prevents the user from collapsing while wearing the device. This also enables the joints to be locked at any point during gait. Requirement 4 is what is needed to move the leg to the equilibrium position. These requirements were calculated using static analysis (Figure 1.9). Because the thigh segment contains no motors and no batteries, its weight should be less than competing devices, which drives Requirement 5. The weight goal is from our previous ESO [24], and it is derived from the weight of the lightest powered orthotic systems.

Table 1.1 - ESO design specifications

No.	ESO Design Specifications		
	Metric	***Unit***	***Value***
1	Lateral width	m	<0.54
2	Seated joint angle hip Seated joint angle knee	Deg Deg	105F 90F
3	Holding torque: hip and knee	Nm	>31
4	Equilibrium torque hip Equilibrium torque knee	Nm Nm	>7.5 >8.2
5	Thigh segment weight	kg	<4.34

Chapter 2. ESO Design

2.1 Structure

The preliminary ESO design for the right leg is shown in Figure 2.1. The left leg is a mirror image. Since we are currently interested in the technical feasibility of the concept, the rest of the orthosis above and below the thigh segment is not shown. Further all of the important joint locking, energy storage and energy release components are located on the thigh segment of the ESO.

Constant force springs were chosen for the energy storing elements. The knee spring and the transfer spring store energy when the quadriceps is stimulated. The hip spring stores energy when the transfer spring is released.

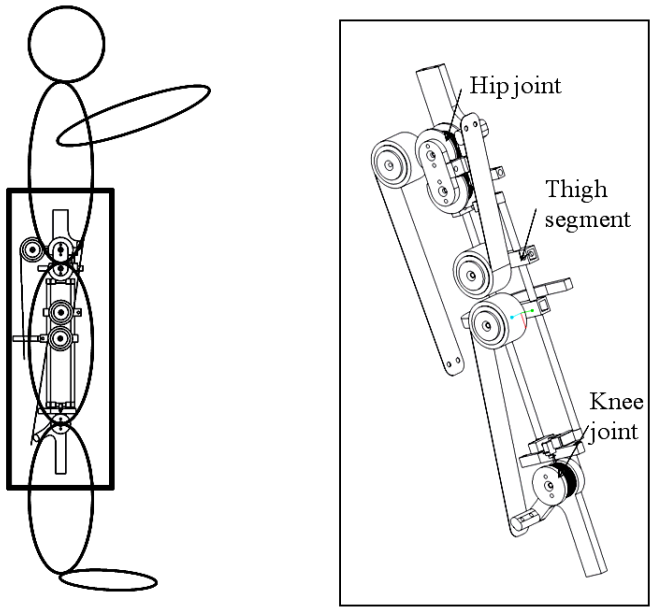

Figure 2.1 - Right leg ESO design. There are three main subsystems the hip joint, the thigh segment and the knee joint.

2.2 Spring Attachment Component

Several components can attach the springs to the joints creating a joint torque. The attachment mechanism determines the torque arm of the joint's torque. Since the torque at the joints varies as the leg is actuated due to gravity, a spring attachment option can be investigated that best accommodates holding the leg at fixed angle positions.

One option is a constant radius pulley. This pulley has a constant joint torque moment arm. Sizes of the circular pulley cannot be changed and require installation of an entirely new pulley in the device. As the size increases, creating a larger torque arm, the energy spring force will decrease, but the stroke length of the spring will increase. When the

pulley diameter decreases the spring force will increase, but the stroke length will get smaller shortening the needed spring displacement. This relationship can be problematic with spring force and displacement capabilities and circular pulleys do nothing to address the varying gravity joint torque.

Another attachment option is a variable radius, or cam pulley. A cam pulley would change radius as the hip and knee joints are actuated. This causes the joint torque to change as hip and knee rotation occurs due to the varying torque arm length. The advantage of the cam pulley is the ability to reduce the torque arm length when a large torque is no longer needed, thus reducing the stroke length of the energy storing spring.

For this project a fixed length bar attachment mechanism was used that combines the function of both pulley types. This option attaches the spring at a specific location on the joint and as the joints are actuated the attachment point will travel in a circular arc motion, but produce a varying torque arm length (Figure 2.2).

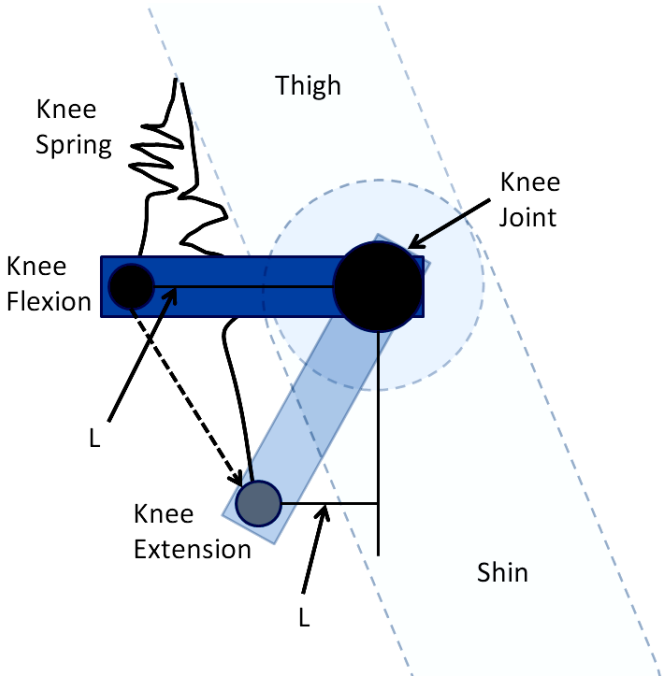

Figure 2.2 – Knee spring attachment bar, L is length of joint torque arm. As the shin rotates the attachment bar rotates displacing the energy storage spring.

The spring attachment bar length can be determined at the flexed equilibrium angles for the hip and knee. This is the angle with the largest gravity torque. The bar length can be calculated by dividing the gravity torque by the spring force at this location. The attachment bars for the knee and hip joints should be installed parallel to the ground at the angle with the highest gravity torque for hip extension and hip and knee equilibrium. Then when the joint is extended from this angle the joint torque moment arm L, will decrease causing the torque on the joint to decrease (Figure 2.2). Because of the torque arm length decreasing during extension the spring joint torque can better match the leg gravity torque profile, unlike the circular pulley. There are several advantages for this

type of spring attachment. Since the component can now be a bar instead of a circular pulley, the weight of this component is reduced. Also no cables that wind around the pulleys are needed, and the spring element can be directly attached to the torque arm bar. Another advantage is the ease of changing the torque arm distance. If more or less torque is needed, based on the ESO user's leg characteristics, the bar length can be changed. This is unlike the cam pulley where a pulley profile has to be determined for an individual user.

2.3 Spring Energy Storage Component

Three springs are incorporated into the ESO design to accomplish gait. Those springs are the knee equilibrium spring, hip equilibrium spring and transfer spring. Springs can be generalized into two categories. Either having a spring constant where the spring force is proportional to the spring displacement, or they have a constant force output. Examples of the first type include coil springs and rubber bands from the previous ESO device. The constant force options include gas springs, or constant force springs. Information on wave springs versus coil springs can be found in the Appendix B.

The energy storing spring for the ESO can be selected by investigating the component joint torque, weight and packaging. To start selecting possible energy storing components the leg gravity torque profiles were revisited (Figure 1.9). The calculated static joint profiles of the two types of springs were plotted with the spring attachment option now

selected. Both types of springs were selected having a force output capable of holding the leg in the equilibrium position. Figure 2.3 shows the joint torque profiles of these two types of springs compared to the joint gravity torque over the knee and hip joint's range of motion.

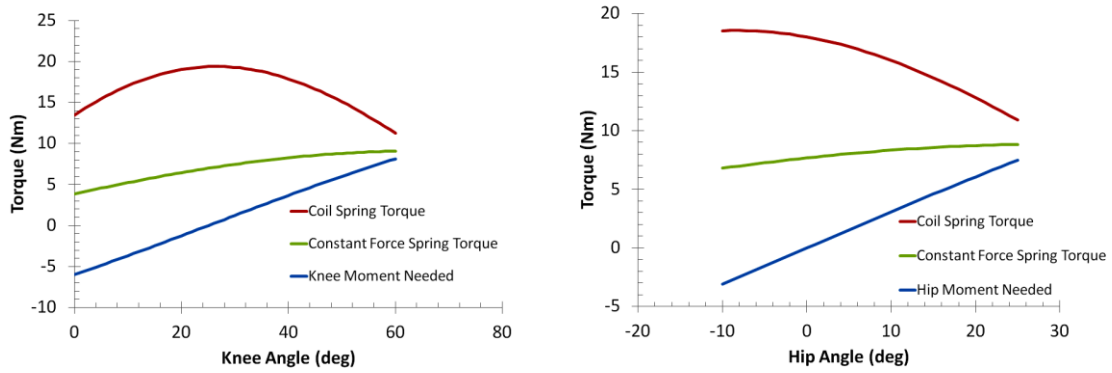

Figure 2.3 - Spring torque profiles for knee and hip joint's range of motion. The two spring types compared to the gravity torque on the joints from the leg's center of mass.

For the coil spring a spring constant was selected from springs capable of meeting the force and displacement requirements of the ESO application. Coil springs do not follow the gravity torque curve as well as the constant force springs indicating that excess energy from the quadriceps will be required to overcome this additional torque. Also as the coil spring displacement increases the force will increase, and for the ESO the torque decreases as the spring is displaced during the hip and knee extension. For this reason the springs whose force is proportional to extension can be eliminated.

The constant force spring torque matches the needed gravity torque better, along with the attachment bar helping to decrease the torque arm length during hip and knee joint extension. This suggests the spring elements for the ESO should be gas springs or constant force springs. Weight and packaging of the energy storage component were further investigated. Constant force springs were chosen for the ESO energy storage components because of component packaging.

If one of the springs can deliver more force per component mass to the ESO the weight of the device would be reduced. Weight is an important design criterion for the ESO and the energy storing springs contain a significant portion of the device's weight. Investigating the difference in weight between the gas springs and the constant force springs (Figure 2.4) reveals that the components have approximately the same force per mass for the component's stroke length. This indicates that either spring is a viable option in the ESO concerning the component weight.

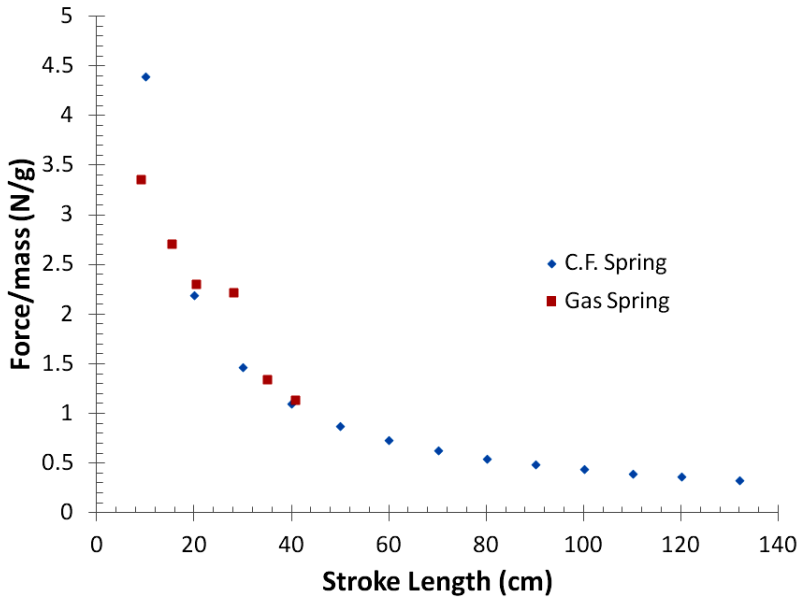

Figure 2.4 - Spring force to weight comparison between a constant force spring and a gas spring

Constant force springs were selected for the ESO because of the packaging capabilities compared to gas springs (Figure 2.5). The difference between the two springs is the extended length. The ratio of the extended length of a constant force spring compared to the stroke length is 1:1. For the gas spring the ratio is 2:1. The cause of this difference is the small length of the constant force spring's housing compared to the stroke length. This is due to the spring coiling around a centralized hub. Unlike the gas spring where the housing has to store the entire stroke length, so when the spring is extended the overall length is double the stroke length. Minimal packaging and size of the energy storing

spring is desired for the ESO, and constant force springs are chosen because the spring extended length is half the size of gas spring's extended length.

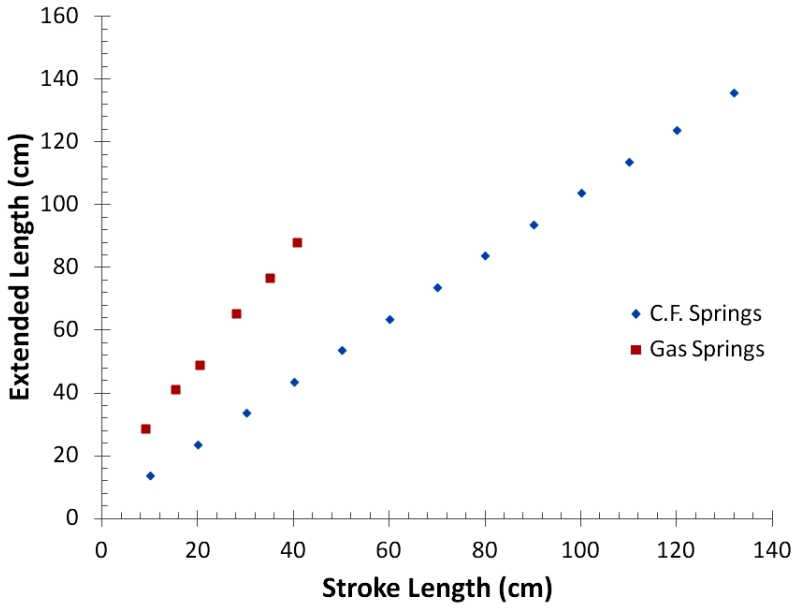

Figure 2.5 - Spring packaging comparison between a constant force spring and a gas spring

2.4 Joint Braking Component

For locking the joints during gait, wrap spring brakes were chosen. Wrap spring brakes work by allowing rotation in one direction, but when locked, not the other (Figure 2.6). Other joint locking options include friction brakes, serrated plates, pin locks, or dog clutches. Wrap springs are advantageous for several reasons. The first is user safety. If power failure of the device occurs the wrap spring unpowered position locks the joint, preventing collapse of the user. Another advantage is the fast unlock/lock response

because the spring can be actuated with just a small motion of the spring's control tang. A third advantage, which is unique to wrap springs, is that the brake can be unlocked under load with only a small force needed to move the spring tang. This means that a small brake actuation mechanism can be used saving space and weight. A fourth advantage is that the wrap spring brake has an exceptional holding torque to weight ratio and a relatively small device can be used to hold the torques seen at the ESO joints when fully loaded.

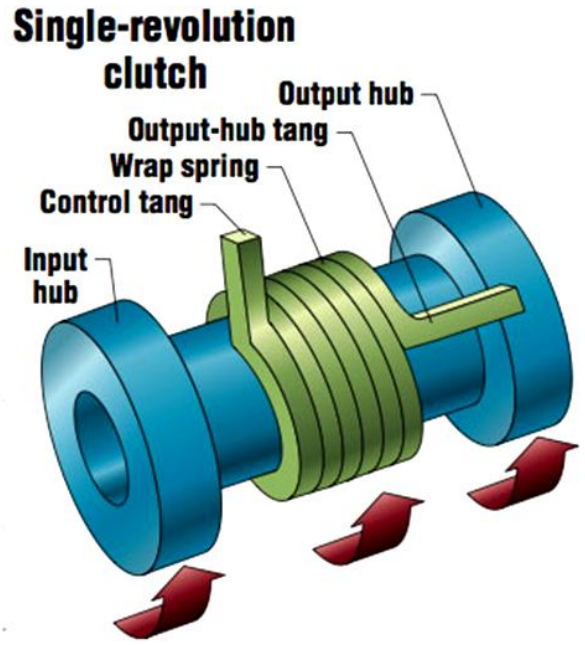

Figure 2.6 - Wrap spring brake, reprinted from http://machinedesign.com/. When locked the input hub can spin in the direction of the arrows, but when the wrap spring control tang is unlocked the input hub can spin in either direction. By attaching the HAT and leg segments to the input and output hubs the joints can be locked and unlocked to prevent and allow joint actuation.

The joint locking torque of the wrap spring was modeled to hold the user in the standing position without collapse. A locking torque greater than 31 Nm was needed and it was determined by static analysis [24]. The wrap springs used for the ESO design have a locking torque of 40 Nm, with the wrap spring torque calculations based on the work of Irby et al. [32]. The wrap spring locking torque equation is

$$T_g = EIR\frac{r-r_0}{r_0 r^2}(e^{2\pi N\mu} - 1)$$

where T_g is the grip torque, R is the shaft radius, r is the neutral axis radius of un-mounted spring, r_0 is the neutral axis radius of mounted spring, N is the number of coil turns and μ is the friction coefficient.

Unlocking the wrap springs requires an actuation mechanism to move the spring's control tang to the unlocked position. Experimental measurements found a control tang displacement of 0.5 cm will completely unlock the wrap spring. The force needed to move the tang 0.5 cm is 4.94 N. More experimental information about wrap spring unlocking can be found in Appendix D.

A mechanical control tang actuation mechanism can be designed knowing the unlocking length and force. The goal of the mechanism is to toggle the wrap spring between the locked and unlocked position, while using the least amount of energy as possible. If possible, the unlocking energy source should be shut off to conserve energy in the

unlocked position since the wrap spring brakes stay unlocked during gait. Possible control tang actuation devices are solenoids, linkages, or motors. For the ESO a servo motor will be used for the actuation mechanism. The advantage of a servo motor is the fast response, control and output force in a small, light device.

A servo motor can be selected from the experimental analysis in Appendix D. For the ESO an achievable servo motor angle of travel, with a reasonable motor arm length, to achieve the fastest control tang actuation time is 60 degrees. The angle of travel cannot be so small that the motor arm length impacts the packaging and size of the joint wrap spring brake system. The Hitec HS-35HD nano servo motor (Figure 2.7) was selected for the size and torque output. The servo motor actuation time is approximately 0.1 seconds for this angle of travel. The torque is approximately 15 Nmm, and the motor arm length is around 5 mm.

Figure 2.7 - Hitec HS-35HD Ultra Nano Servo Motor, reprinted from http://www.servocity.com/

2.5 Hip Joint Design

The hip joint is shown in Figure 2.8. Energy storing in the transfer spring from the quadriceps takes place in a constant force spring. The connection for the hip equilibrium spring is also located on the hip joint. The attachment points of the springs were selected to provide the desired joint torques. Two wrap springs with servo motors are embedded in the hip joint wrap spring brake. The joint reflects effort in making the width and overall profile as minimal as possible.

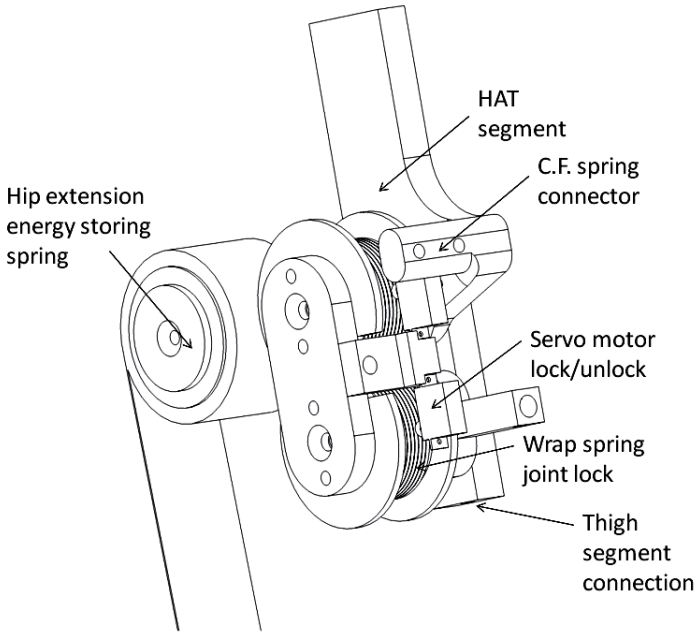

Figure 2.8 - Hip joint design

Hip Joint Locking System

A custom wrap spring brake is used to lock the hip joint. With ESO gait, during certain phases, the hip must not rotate in either direction so two coupled wrap spring brakes are used. Shafts hold the two wrap springs, and 2024 aluminum alloy gears transfer the motion between the two brakes (Figure 2.9). This concept works by the gears switching the direction of rotation between the two shafts, and locking of identical wrap springs allow no rotation. A key aspect of this design is locking the hip joint in both directions required no added hip width; instead the second wrap spring was added parallel to the thigh.

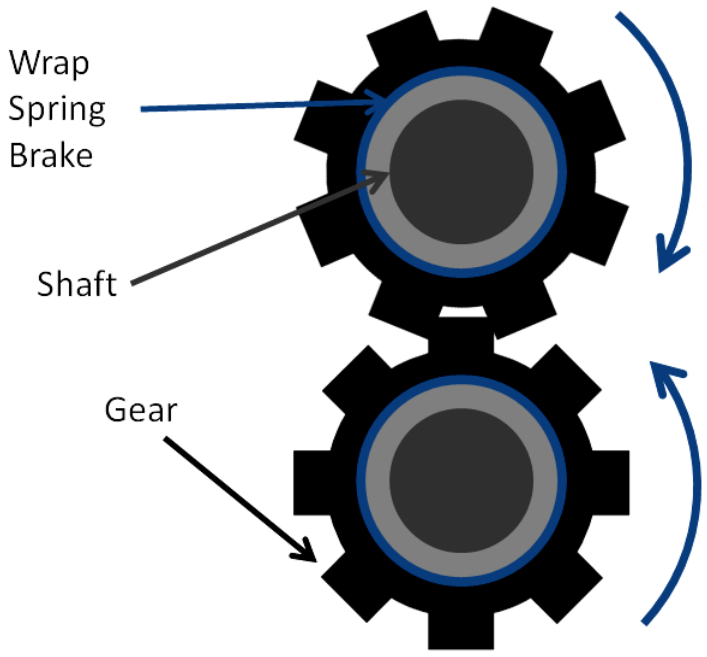

Figure 2.9 - Hip braking concept. The top input gear causes the rotation of the bottom gear to reverse, creating two shafts rotating in opposite directions that can now be locked in both directions by two identical wrap springs.

Gear Analysis

This section explains how the gear width is determined in the ESO hip joint. A width can be found by calculating the gear factor of safety. The minimum gear width will reduce the weight and width of the hip joint. The hip will be the widest section of the ESO device, so finding the minimal gear width is important.

A spur gear was selected to complete the locking and unlocking of the hip joint (SDP/SI, S1086Z-024A045). The gear diameter must provide enough operating clearance between the two wrap springs located at the hip joint. A gear with a pitch diameter of 1.88 in was selected for this reason.

Analysis of the gear is modeled from Juvinall and Marshek [33]. This equation for finding the tooth bending stress is

$$\sigma = \frac{F_t P}{bY}$$

where F_t is the tangential component of the gear force, P is the diametral pitch, b is the gear width, and Y is the Lewis form factor. The safety factor equation is

$$S.F. = \frac{S_n}{\sigma}$$

where S_n is the fatigue strength of the gear material. The smallest width can be selected by the safety factor calculations for different widths.

Gear safety factor results are in Figure 2.10. The x-axis value is the gear width. The widths range from 0.1 in. to 0.5 in. The resulting safety factors range from a minimum of 1 to a maximum of 5.25. As the gear width increases the safety factor increases linearly.

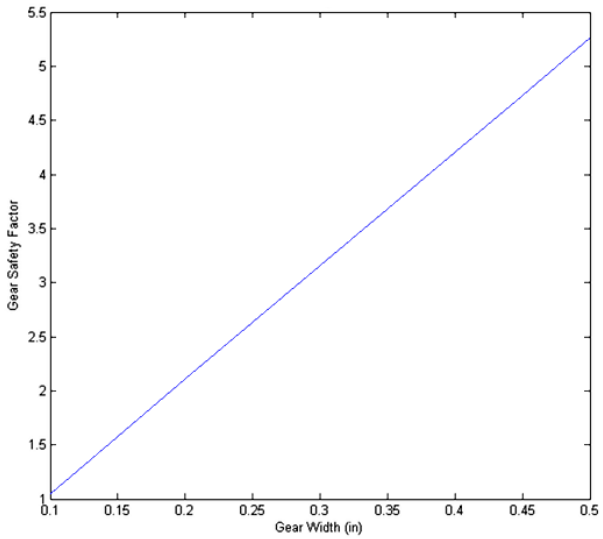

Figure 2.10 - Gear width safety factor for a range of gear widths from 0.1 in. to 0.5 in.

A suitable gear width can be selected by analyzing Figure 2.10. Usual engineering applications ask for a safety factor of 2. Any width value from 0.1 in. to 0.2 in. is unacceptable for the ESO design. At just over 0.2 in. the safety factor is 2.1. This would be acceptable for the device, but does not account for any unforeseen problems that could

cause the gear to fail. Instead, a gear width of 0.25 in. was selected. The resulting safety factor is 2.6.

2.6 Thigh Beam Design

The thigh segment (Figure 2.11) provides the device structural support, fixation and housing for the mechanical hardware while coupling the hip and knee joints. Structural support of the thigh segment is provided by two 6061 aluminum tubes sized to support the loads from the energy storage components while remaining rigid to prevent bending. The weight of the device was reduced by using tubes instead of solid rod members. Another support member is the under the leg support bar also made from 6061 aluminum, and works to stabilize the leg along with the straps. The thigh segment houses the hubs of the hip and knee equilibrium constant force springs. They are placed in the middle of the thigh segment to minimize the profile and size.

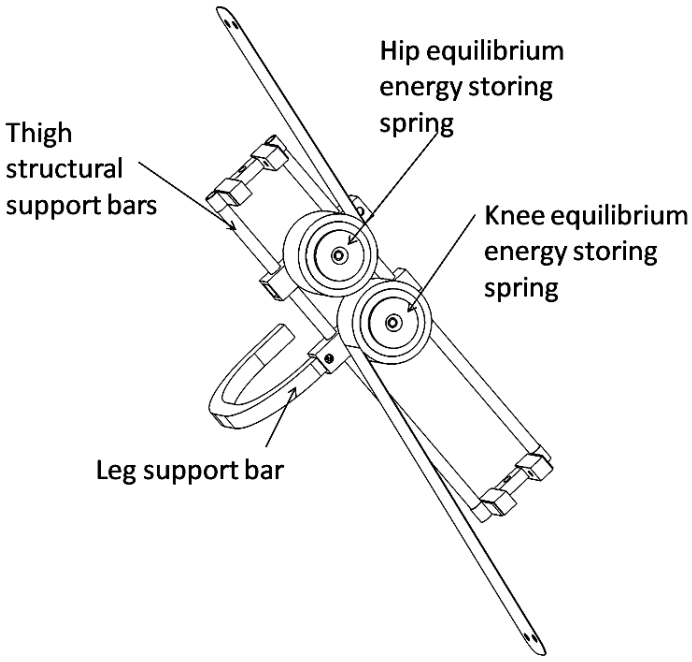

Figure 2.11 - Thigh segment design that connects the hip and knee joints

The smallest beam diameter to use in the thigh segment can be determined. An acceptable diameter will be determined by calculating the beam factor of safety and the deflection. Since the thigh beams are long any reduction in diameter will significantly reduce the weight of the device.

Figure 2.12 - Thigh beam free body diagram. Energy storage elements try to rotate the beam, but support from the leg support bar and hip joint prevents rotation.

The thigh beam can be modeled as a simple beam (Figure 2.12). T_{hip} and T_{knee} are the torques at the hip and knee joints. $F_{support}$ is the reaction force of the moments at the location of the leg support bar. The force of the support bar can be found by setting the sum of the moments equal to zero at the hip location. The support bar force equation is

$$F_s = \frac{T_h + T_k}{D_s}$$

where D_s refers to the distance of the support bar from the hip. The thigh beam's factor of safety can be calculated by dividing the beam material's shear strength by the stress on the thigh beams. The beam stress is found by dividing the force of the support bar by the area of the beams.

The deflection of the beams is the other important calculation. The desired joint angles will not be reached if deflection of the thigh beams is allowed in this application. The

deflection model incorporates the beams from the hip to the knee joint with an intermediate load, the support bar force, with two simple supports. The deflection equation is

$$\delta = \frac{Fa^2(L-a)^2}{3EIL}$$

where F is the force of the support bar, a is the distance of the support bar from the hip, L is the length of the beam, E is Young's Modulus of the beam material, and I is the moment of inertia [34]. The factors of safety and deflections can be determined using these equations for different beam diameters. Then a beam diameter with minimum deflection can be selected for the ESO application.

The beam ranges from 0.125 in. to 0.5 in. The safety factors of the beams are well above the minimum for the ESO thigh segment. The beam deflection is of most concern because any beam deflection will prevent the joints from reaching the desired joint range of motion. Beam deflection results are in Figure 2.13.

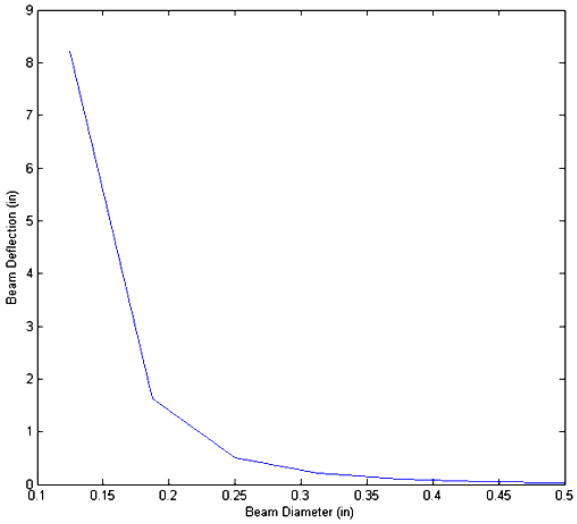

Figure 2.13 - Thigh beam deflection for a range of available beam diameters ranging from 0.125 in. to 0.5 in.

Any beam diameter that deflects more than 0.5 in. is unacceptable for the ESO device. A beam diameter of 0.375 in. will satisfy the deflection criteria based on the standard sizes of rod diameters. At this beam diameter the deflection is 0.1 in., which is minimal. This thigh beam diameter should provide an adequate design for the ESO device by minimizing deflection and weight.

2.7 Knee Joint Design

The knee joint (Figure 2.14) is similar to the hip joint in materials, components and function. One difference is the need to lock knee rotation in only one direction, which means there is a single wrap spring and servo motor at the knee for joint braking. Extension rotation is always allowed because the quadriceps stimulation can be turned off and the knee will no longer rotate in that direction due to energy stored in the knee

equilibrium spring. The knee spring is connected to the knee joint at a desired torque arm length to generate the needed torque for holding the joint in the equilibrium position.

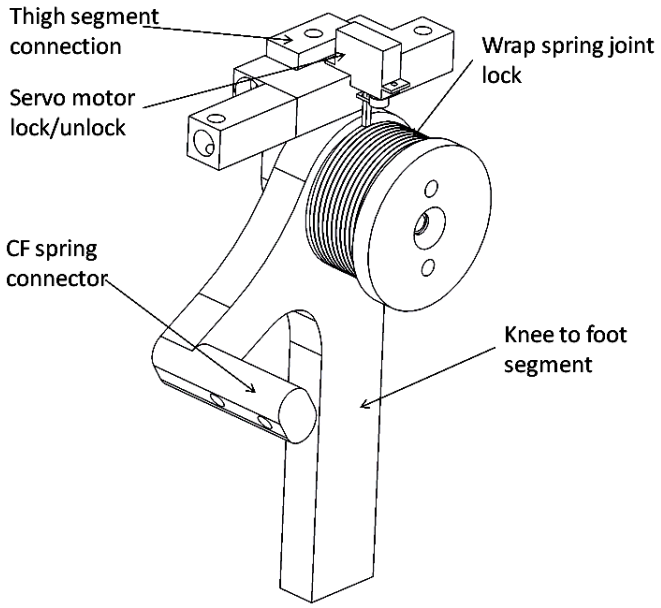

Figure 2.14 - Knee joint design

Chapter 3. ESO Assessment

3.1 Thigh Prototype

The thigh prototype (Figure 3.1) was created for experimental assessment of the ESO. The three constant force springs are connected by bolts to the attachment bars located at the hip and knee joints. Three wrap springs are used to lock and unlock the hip and knee joints along with three servo motors. Support rods on the thigh segment help to stabilize the device and house the equilibrium constant force springs. Further details on the prototype are in Appendix E.

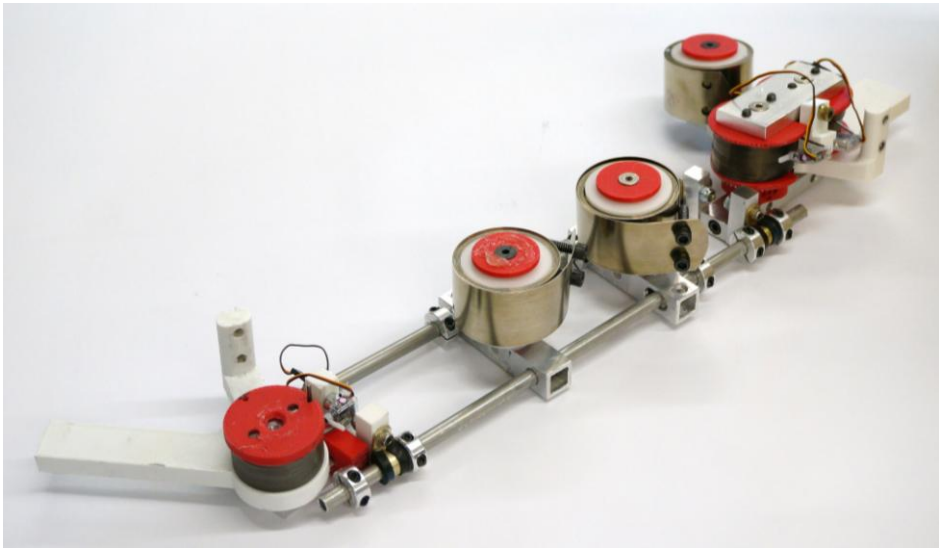

Figure 3.1 - ESO thigh prototype. Constant force springs not loaded to attachment bars because force on joints is high without the gravity torque from leg.

3.2 Objective

Dynamic Simulation

A dynamic simulation model was used to evaluate the gait dynamics of the ESO design. Simulations of the different phases of the gait sequence will give useful data on the available energy, joint positions, and timing of the proposed design. This data will help evaluate the feasibility of the ESO design.

Examining the dynamics of leg movement during each of the gait phases can determine whether the energy storage elements are acting as intended. Another purpose was determining the timing to complete each phase of the gait cycle. The gait cycle time of the design could be proven impractical if the cycle time is slow compared to the non-impaired gait time of 1 cycle/second.

Bench-top Testing

Static and dynamic data will be collected for the prototype. The objective of testing the prototype is to evaluate feasibility of the ESO concept in accomplishing gait. The other importance for performing bench-top testing is to compare the data to the simulation predictions. Analysis will verify whether the simulation is a useful tool and the prototype components are functioning as predicted in the simulation. The bench-top set-up is shown in Figure 3.2.

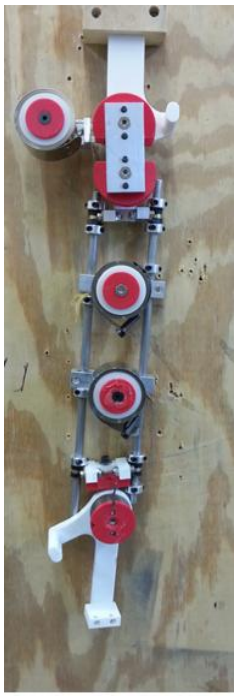

Figure 3.2 - ESO bench-top testing set-up. Thigh prototype mounted vertically to plywood so gravity can be properly accounted for.

3.3 Methods

Dynamic Simulation

The dynamic simulation model was implemented using Matlab and SimMechanics. The leg of an average male and the ESO device worn on the leg were modeled as a two link mechanism with the proper mass and center of gravity [30], [31]. Forces, torques and spring components were attached to these linkages to model the stimulation of the quadriceps and the energy storage components. The thigh and shin lengths were both 0.43 m and the mass was 8 kg and 3.7 kg respectively. The force from the energy storage elements was 107 N.

The simulations give analytical results and are also shown as animations to insure desired dynamic performance. Solid body members were defined, in this case the leg linkages, in the block diagram for the ESO simulation. Then parameters were applied to the solid bodies resembling the dynamic forces and joints that are in the system. Pin joints were used to connect the solid model linkages in the simulation.

The hip and knee joints were modeled as revolute joints, and the initial starting position of the joints and the allowable actuation angles were specified. Then forces from the constant force springs were defined and attached to the model with proper positioning on the linkages to simulate the realistic attachment and operation of the energy storing components. To simulate the quadriceps FES torque, a joint input torque was applied to the knee joint. The simulation will be useful in determining what the magnitude of the quadriceps input torque will be to accomplish gait and if it is below the available quadriceps torque [16]. The quadriceps minimum torque will be found by finding the value where the gait phases can no longer be completed due to lack of energy storage. More information on SimMechanics simulations is in Appendix E.

There are three phases of interest during the gait cycle for the dynamic simulations. The first is the quadriceps stimulation phase. The purpose of this simulation is to determine the required quadriceps torque to drive the gait cycle and to investigate the dynamics of the joint angles as a function of time. If the energy storing components used to complete

the gait cycle require too much torque from the quadriceps, rapid muscle fatigue will occur and the design would be impractical. The next simulation is the hip extension phase which explores the hip extension timing and positioning for the joint range of motion. Then the return to the equilibrium position of the hip and knee joints can be simulated investigating the position and timing. The simulations start and finish positions of the knee extension, hip extension and return to equilibrium gait phases are in Figure 3.3.

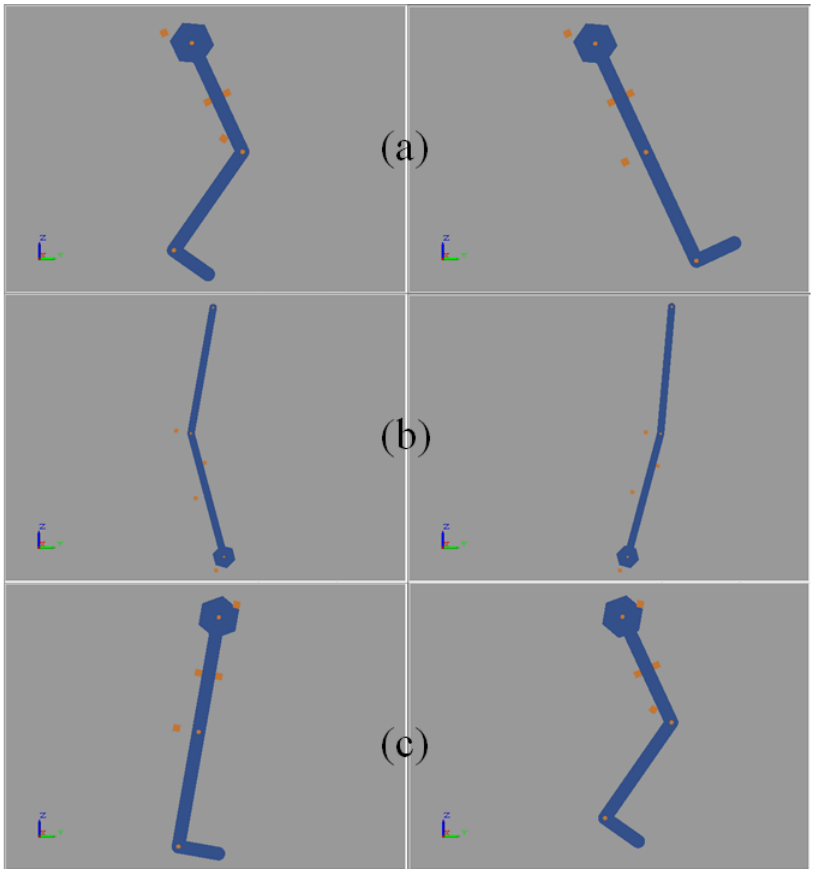

Figure 3.3 - Simulation phases start to finish. (a) is the knee extension simulation to full knee extension. (b) is the hip extension system, and (c) is the return to equilibrium.

The simulation animation displays the linkages and the blocks (Figure 3.3) represent the constant force spring attachment points. In the knee extension and equilibrium simulations the thigh, lower leg and foot were modeled by the linkages. The fixed point was at the hip joint. Whereas with the hip extension the entire leg was modeled as a linkage and the upper linkage is the HAT segment. The bottom of the leg linkage, which is in contact with the ground, is the fixed point for this simulation.

Bench-top Testing

A preliminary prototype of thigh segment was created. Weights were placed on the thigh segment and shin segment of the prototype matching the mass and center of gravity of the average leg [30], [31].

The static torque of the hip and knee joints was measured using a tension force sensor (Wagner Instruments, Force Five). A force gage was used to measure the joint force for the hip and knee joint's range of motion. Three trials were conducted at each joint. Force was recorded in angle increments of 5 degrees using a protractor at the joints that connected to the leg segments. This force data can then be converted to a torque by multiplying the torque arm length where the force was measured.

A motion capture camera and subsequent programming was used to measure the dynamic data for the ESO prototype. This data gives useful information on the joint positioning and timing that can be compared to the simulation data.

The motion capture system that was used is a motion capture camera (Basler, Scout) in conjunction with video recording software (Pylon Viewer). This software sets video recording parameters for the prototype testing. Motion analysis software (Innovision Systems, MaxTRAQ) was used to analyze the video. Retro reflective markers were placed on the hip and knee joints, the HAT and shin segments of the prototype for the motion capture analysis. Points on the prototype can be defined in the software and joint angles formed by these points can be calculated as the prototype test video is advanced (Figure 3.4). More information about the motion capture system and software can be found in Appendix G.

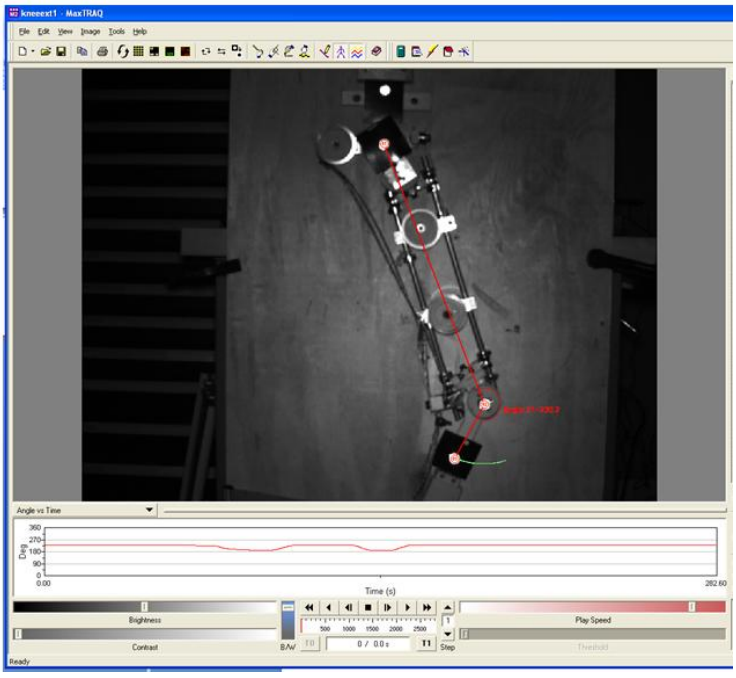

Figure 3.4 - MaxTRAQ motion capture software. Video can be played and stopped while tracking joint angles. The program can plot the angles for the testing time.

There are three phases of interest during the gait cycle for the dynamic prototype testing. These are identical to the phases used in the dynamic simulation. The first is the quadriceps stimulation phase. From this knee extension actuation time can be found. The hip extension phase timing is the next simulation. The return to equilibrium position timing is the last test phase. For each phase of gait 10 test trials were conducted for dynamic prototype testing.

3.4 Results

Design Requirements

The thigh prototype and the computer solid model were used to verify the size and weight requirements specified for the ESO (Table 3.1). The overall width of the design is 0.505 m while still accommodating the hip width of the average adult male. This is below the specification for allowing the user of the device to fit into a wheelchair when sitting down. The ESO thigh prototype mass is 2.33 kg and was estimated to be 2.5 kg from the solid model design, which is under the requirement for the leg. Weight for orthotic bracing above the hip joint and below the knee joint will still need to be added to secure prototype to a leg, but most of the weight will still be in the energy storage components in the thigh segment of the device. More weight can even be removed from the prototype components, and more information is in Appendix H. Further, while not a requirement, the joint is compact, extending only 0.032 m above the hip and 0.025 m below the knee.

Table 3.1 - ESO design requirement results

No.	ESO Design Specifications			
	Metric	***Unit***	***Required***	***Measured***
1	Lateral width	m	<0.54	0.505
2	Seated joint angle hip Seated joint angle knee	Deg Deg	105F 90F	105 90
3	Holding torque: hip and knee	Nm	>31	40
4	Equilibrium torque hip Equilibrium torque knee	Nm Nm	>7.5 >8.2	20 16
5	Thigh segment weight	kg	<4.34	2.33

Static Joint Torque

Static force measurements were taken at both joints. The force on the joints will be due to excess energy needed for joint actuation stored in the springs greater than the joint torque due to gravity. The results are in Table 3.2 and Table 3.3. This force data can then be converted to a joint torque in Figure 3.5.

Table 3.2 - Static hip joint torque

Hip joint force vs. knee angle									
	Hip angle (deg)	*-10*	*-5*	*0*	*5*	*10*	*15*	*20*	*25*
Hip force (N)	Trial 1	48	46	37	27	20	12	4.4	0
	Trail 2	48	42	38	29	22	18	8	0
	Trial 3	49	47	39	27	19	15	7.6	0

Table 3.3 - Static knee joint torque

Knee joint force vs. knee angle														
	Knee angle (deg)	*0*	*5*	*10*	*15*	*20*	*25*	*30*	*35*	*40*	*45*	*50*	*55*	*60*
Knee force (N)	Trial 1	57.8	47.2	43.1	40.0	36.5	33.4	29.8	25.4	20.9	22.2	15.1	8.9	2.7
	Trail 2	57.8	45.4	44.0	40.0	37.4	32.5	31.6	24.9	20.0	16.5	12.5	8.0	2.7
	Trial 3	57.4	54.7	43.6	38.3	36.9	33.8	29.8	25.8	21.8	17.3	12.9	8.9	2.7

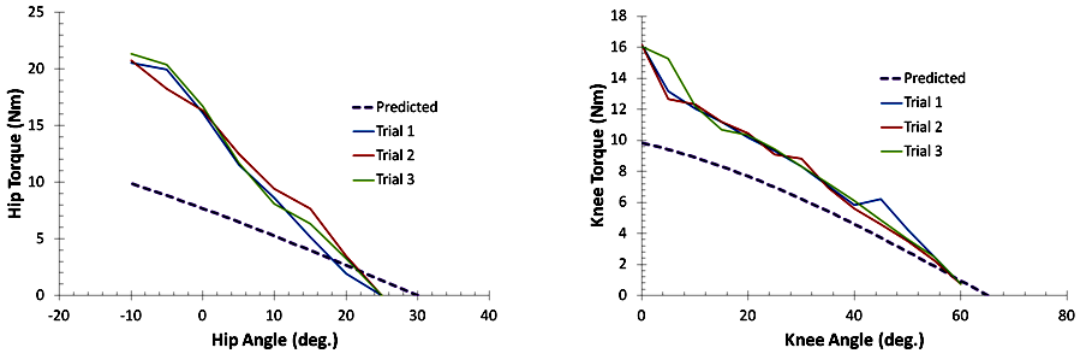

Figure 3.5 – Hip and knee static joint torque data. This data is the excess torque on the joints due to the energy storing springs. The predicted excess energy from initial static calculations is the dotted line.

For both of the joints the maximum torque was at full extension, and the minimum occurs at the equilibrium angles of flexion. For the hip the maximum measured torque was 20 Nm and the predicted was 10 Nm, and for the knee the maximum was 16 Nm and the predicted was 10 Nm.

Dynamic Testing

The knee extension phase actuates the knee joint from the angles of -60 degrees to 0 degrees with 0 degrees referring to full knee extension. When knee extension occurs the quadriceps muscle provides energy that is stored in the equilibrium spring and the transfer spring. A quadriceps torque of 15 Nm was implemented for the trials, which is below the available quadriceps' stimulation torque [16]. The knee extension test interest was the amount of time for the knee joint to fully extend. Figure 3.6 shows the knee joint

angle versus time. The simulation time to extend the knee using FES of the quadriceps was 0.68 sec. The average time of the trails to extend the knee was 0.97 sec.

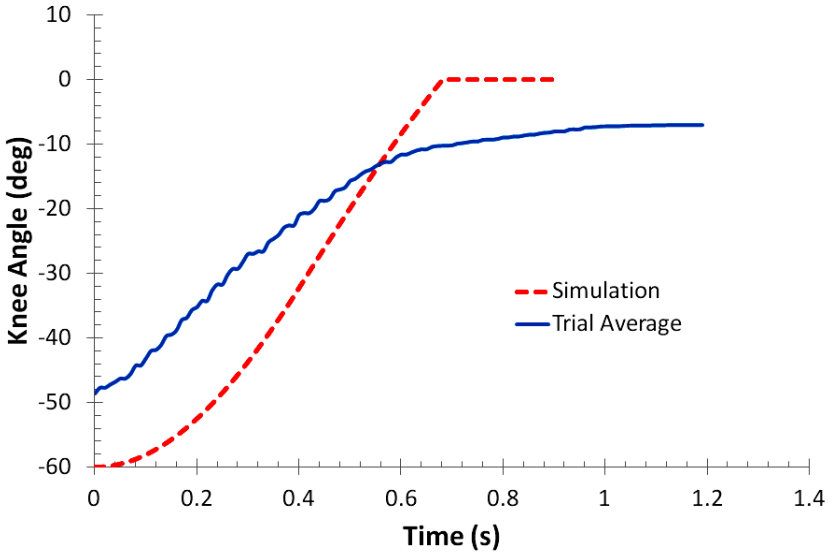

Figure 3.6 - Knee extension trials

Hip extension is the next phase test results. The hip was actuated from 25 degrees to -10 degrees. The individual trial results of the hip extension actuation are in Figure 3.7. All other trial results are averaged when presented as results. Figure 3.8 shows the average of the trials. The hip extension phase took 0.22 sec for the simulation, and the average motion capture hip extension trial time was 0.24 sec.

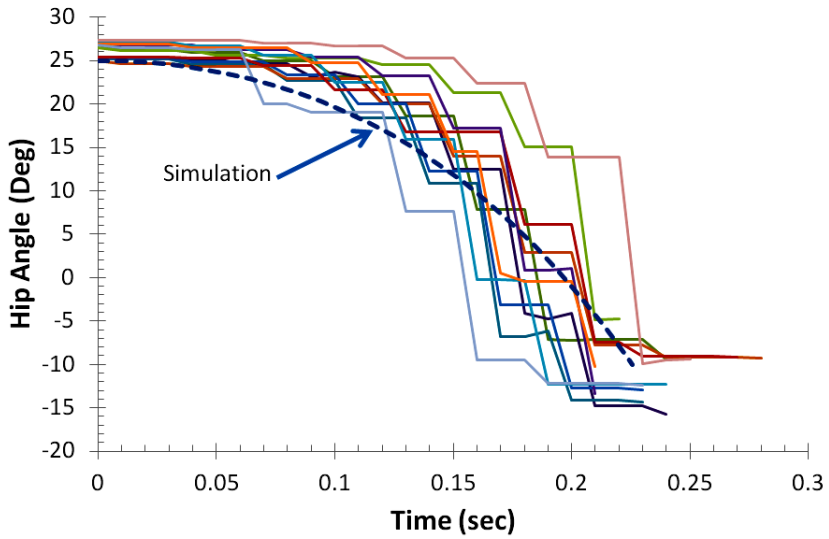

Figure 3.7 – Individual hip extension trials. Simulation prediction comparison is the dotted line.

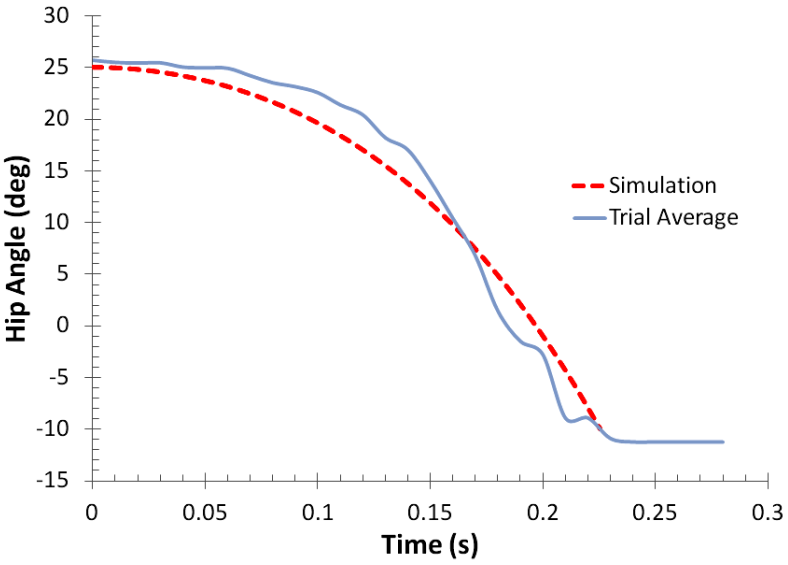

Figure 3.8 - Hip extension trials

The final dynamic testing phase is the return to the equilibrium position. The knee angle returned from 0, full knee extension, to -60 degrees and the hip angle returned from -10 to 25 degrees. Hip equilibrium dynamic results are in Figure 3.9. The time of the hip equilibrium trials was 0.72 sec, and the hip simulation time was 0.36 sec.

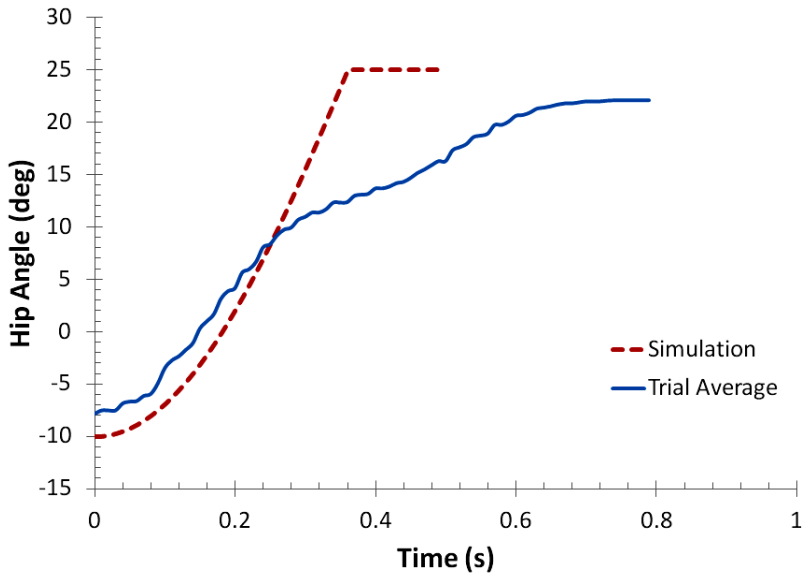

Figure 3.9 - Hip equilibrium trials

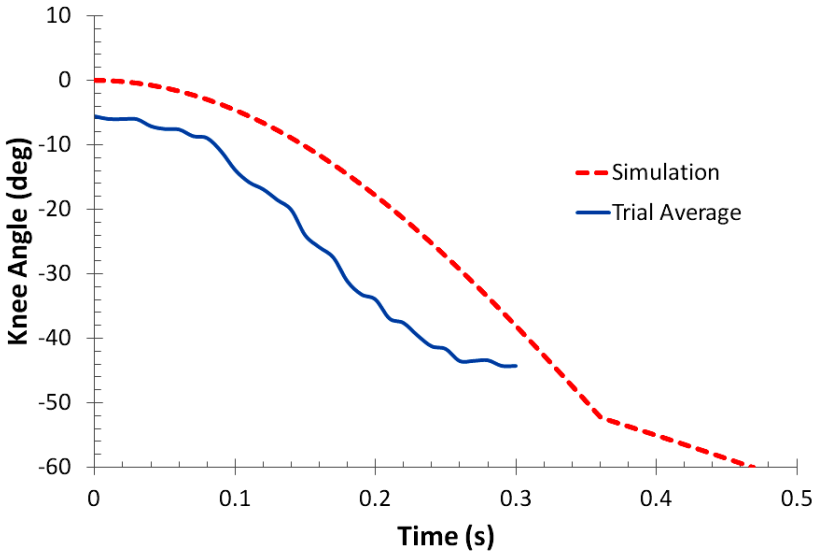

Figure 3.10 - Knee equilibrium trials

The return to equilibrium position for the knee joint is in Figure 3.10. The average trial time for the knee to reach equilibrium was 0.24 sec. The simulation predicted this time to be 0.47 sec.

Results and analysis of the gait phase data are available in Table 3.4. The percent error was used to compare the simulation time and mean trial time. The root mean square deviation (RMSD) calculation compares the predicted simulation profiles and the actual trial profiles. The RMSD averages the mean difference squared between the simulations and trials for the time increments of the motion capture system. Then the square root of

the difference average is taken giving a standard deviation in degrees between the predicted and experimental profile values.

Table 3.4 - Dynamic results

	Knee Extension	*Hip Extension*	*Hip Equilibrium*	*Knee Equilibrium*
Simulation Time (s)	0.68	0.22	0.36	0.47
Avg. Trial Time (s)	0.97	0.24	0.72	0.24
Standard Deviation (s)	0.13	0.02	0.04	0.04
% Error	42.65%	8.04%	98.61%	48.67%
RMSD (deg)	11.23	0.65	2.13	5.56

The total single leg gait based on the dynamic simulations was 1.37 sec. To complete the entire gait sequence involving the other leg the time would be 2.74 sec. For the prototype trials the single leg gait time was 1.92 sec, and the entire gait sequence would take 3.84 sec.

3.5 Discussion

Determining if the ESO design is feasible for producing gait is the main purpose of assessing the prototype and concept. For the ESO to be feasible the design must be able to complete the different stages of the gait cycle using only the energy from the quadriceps muscle. Also the design must uphold the design requirements for use and functionality, and the cycle time to complete gait must be reasonable compared to other gait devices.

The static joint torque results (Figure 3.5) indicate that the energy storing springs are capable of holding the leg at any angle needed for the joint's range of motion. Our design requirement results demonstrate the prototype meets all of the design targets (Table 3.1).

If the joint gravity torque could be matched precisely by the energy storing springs the measured static torques would be just above zero (Figure 3.5). Based on previous spring torque profile analysis (Figure 2.3) this is not the case for the constant force springs and extra torque will be created compared to the gravity torque.

The measured static torque data is higher than the predicted values. This could cause knee and hip extension to take longer than predicted by the simulation. Both of the measured joint torques act as expected for releasing energy for completing the gait phases.

The dynamic testing indicates that gait can be completed using the ESO for all phases: knee extension, hip extension and return to equilibrium. Our experimental results of gait timing differ from the simulation predicted times (Table 3.4).

Figure 3.6, Figure 3.8, Figure 3.9 and Figure 3.10 demonstrate that the gait phases are being completed by the ESO. The profiles show that the joint angles are actuating in the desired direction with the proper timing indicating concept feasibility. The root mean square deviation results suggest that these profiles are similar between the ESO prototype

and simulation data. For some of the testing phases the joint angles are not able to reach their desired joint range of motion impacting the similarity between the trials and the simulations and thus the root mean square deviation values. Bending where the joint attaches to the thigh segment is the cause for this problem. The root mean square deviation values for the knee joint are higher and bending was apparent at this joint during testing compared to the hip joint.

The timing of the gait phases is shown in Table 3.4. The percent error results show that the chance of the trial timings being related to the simulation timings is minimal, except with the hip extension trial with an 8% error. The hip and knee equilibrium results show the largest RMSD and percent error. The testing times are slower than the simulation times for the knee extension, hip extension and hip equilibrium. The cause could be friction in the joints that are not accounted for in the simulation. Also the higher than predicted static joint torque results may account for the slower phase times.

One implication of the ESO assessment is that the concept can complete the gait cycle phases. What this indicates is the main components of the ESO design are viable options. These are the constant force springs used for storing and releasing energy, and the wrap springs used to lock and unlock the joints. The other implication from the ESO assessment is the time to complete the gait sequence. The cycle time was 3.84 sec based on prototype trials. This is slower than conventional gait, but similar to the gait cycle

times of other available gait restoration devices. This cycle time is influenced by the minimal quadriceps torque input of 15 Nm. If the torque is increased to the average available torque, 53 Nm, the gait time would be reduced during the knee extension phase.

3.6 Conclusion

The ESO is a new hybrid orthosis concept for restoring walking to people with spinal cord injury. The main components of the design were found to be the energy storing and joint locking components. Three constant force springs were selected and used for storing energy that drive hip extension and the return to equilibrium of the hip and knee joints. Stimulation of the quadriceps uses 15 Nm of torque to drive knee extension and provide energy to the constant force springs. Wrap spring brakes at the hip and knee joints were chosen to be the joint locking components for their advantageous size and functionality. Two wraps springs were used at the hip joint to lock rotation in both directions, and one wrap spring was used at the knee joint allowing rotation in the knee extension direction only caused by FES of the quadriceps.

The purpose of the project was to create a new ESO concept. Assessment of the main components of the ESO design reveals that the device should be feasible for accomplishing gait. Analysis of the ESO feasibility occurred during the concept, simulations and testing phases of the project. Concept analysis showed that the main components should act together with systematic timing to accomplish gait. Dynamic

simulations indicated the components could work together to complete the different gait phases. The simulations provided timing and positioning data. Then a prototype was created for bench-top testing. Prototype construction and testing verified the design requirements, static and dynamic feasibility and an acceptable gait cycle time.

One need for the ESO device is the ease of donning and doffing the device for the user. Use of this device by people with SCI will require them to be able to independently use the device including taking it on and off. Further development is needed to achieve a good way for the user to easily get into and out of the orthotic bracing of the ESO. The advantage of the thigh ESO design is that the thigh component can be independent of the orthotic bracing so the device can be assembled with several lighter components. Another need is hip and knee joint stops. These joint stops allow the joint's range of motion during gait, but prevent the joints from reaching angles outside the range of motion. Then when sitting is desired these stops can snap out of place so the hip and knee can flex past the range of motion needed during gait. Ideally when the user stands up from the wheelchair the stops will snap back into place automatically and gait can be continued. Figure 3.11 is a rendering of how the final ESO could look. No bracing or components are located on the inside of the legs making the device easier to don and doff.

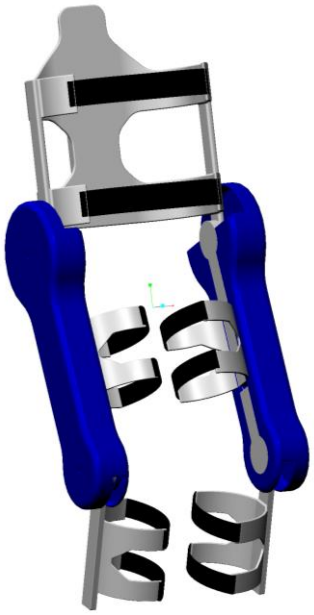

Figure 3.11 – Possible ESO final product

References

[1] D. L. Brown-Triolo, M. J. Roach, K. Nelson, and R. J. Triolo, "Consumer perspectives on mobility: implications for neuroprosthesis design," *J. Rehabil. Res. Dev.*, vol. 39, no. 6, pp. 659–669, Dec. 2002.

[2] Peter W. Axelson and D. R. G. Ann Lasko Harvill, "Standing and its importance in spinal cord injury management," *Proc. RESNA 10th Annu. Conf.*, pp. 477–479, 1987.

[3] "The 2012 Annual Statistical Report for the Spinal Cord Injury Model Systems," National Spinal Cord Injury Statistical Center, 2012.

[4] H. Herr, "Exoskeletons and orthoses: classification, design challenges and future directions," *J. Neuroengineering Rehabil.*, vol. 6, p. 21, 2009.

[5] G. H. Creasey, C. H. Ho, R. J. Triolo, D. R. Gater, A. F. DiMarco, K. M. Bogie, and M. W. Keith, "Clinical applications of electrical stimulation after spinal cord injury," *J. Spinal Cord Med.*, vol. 27, no. 4, pp. 365–375, 2004.

[6] P. J. Pacy, R. H. Evans, and D. Halliday, "Effect of anaerobic and aerobic exercise promoted by computer regulated functional electrical stimulation (FES) on muscle size, strength and histology in paraplegic males," *Prosthet. Orthot. Int.*, vol. 11, no. 2, pp. 75–79, Aug. 1987.

[7] R. Turk and P. Obreza, "Functional electrical stimulation as an orthotic means for the rehabilitation of paraplegic patients," *Paraplegia*, vol. 23, no. 6, pp. 344–348, Dec. 1985.

[8] D. Guiraud, C. Azevedo Coste, M. Benoussaad, and C. Fattal, "Implanted functional electrical stimulation: case report of a paraplegic patient with complete SCI after 9 years," *J. Neuroengineering Rehabil.*, vol. 11, no. 1, p. 15, Feb. 2014.

[9] K. T. Ragnarsson, "Physiologic effects of functional electrical stimulation-induced exercises in spinal cord-injured individuals," *Clin. Orthop.*, no. 233, pp. 53–63, Aug. 1988.

[10] G. A. Wu, L. Lombardo, R. J. Triolo, and K. M. Bogie, "The effects of combined trunk and gluteal neuromuscular electrical stimulation on posture and tissue health in spinal cord injury," *PM R*, vol. 5, no. 8, pp. 688–696, Aug. 2013.

[11] J. A. Davis Jr, R. J. Triolo, J. P. Uhlir, N. Bhadra, D. A. Lissy, S. Nandurkar, and E. B. Marsolais, "Surgical technique for installing an eight-channel neuroprosthesis for standing," *Clin. Orthop.*, no. 385, pp. 237–252, Apr. 2001.

[12] J. P. Uhlir, R. J. Triolo, and R. Kobetic, “The use of selective electrical stimulation of the quadriceps to improve standing function in paraplegia,” *IEEE Trans. Rehabil. Eng. Publ. IEEE Eng. Med. Biol. Soc.*, vol. 8, no. 4, pp. 514–522, Dec. 2000.

[13] M. L. Audu, R. F. Kirsch, and R. J. Triolo, “Experimental verification of a computational technique for determining ground reactions in human bipedal stance,” *J. Biomech.*, vol. 40, no. 5, pp. 1115–1124, 2007.

[14] E. Marsolais and R. Kobetic, “Functional electrical stimulation for walking in paraplegia,” *J. Bone Jt. Surg.*, vol. 69, no. 5, pp. 728–733, Jun. 1987.

[15] R. Kobetic, R. J. Triolo, and E. B. Marsolais, “Muscle selection and walking performance of multichannel FES systems for ambulation in paraplegia,” *IEEE Trans. Rehabil. Eng.*, vol. 5, no. 1, pp. 23–29, Mar. 1997.

[16] J. M. Hausdorff and W. K. Durfee, “Open-loop position control of the knee joint using electrical stimulation of the quadriceps and hamstrings,” *Med. Biol. Eng. Comput.*, vol. 29, no. 3, pp. 269–280, May 1991.

[17] H. A. Quintero, R. J. Farris, C. Hartigan, I. Clesson, and M. Goldfarb, “A Powered Lower Limb Orthosis for Providing Legged Mobility in Paraplegic Individuals,” *Top. Spinal Cord Inj. Rehabil.*, vol. 17, no. 1, pp. 25–33, 2011.

[18] R. J. Farris, H. A. Quintero, and M. Goldfarb, “Preliminary evaluation of a powered lower limb orthosis to aid walking in paraplegic individuals,” *IEEE Trans. Neural Syst. Rehabil. Eng. Publ. IEEE Eng. Med. Biol. Soc.*, vol. 19, no. 6, pp. 652–659, Dec. 2011.

[19] A. Esquenazi, M. Talaty, A. Packel, and M. Saulino, “The ReWalk powered exoskeleton to restore ambulatory function to individuals with thoracic-level motor-complete spinal cord injury,” *Am. J. Phys. Med. Rehabil. Assoc. Acad. Physiatr.*, vol. 91, no. 11, pp. 911–921, Nov. 2012.

[20] S. Gharooni, B. Heller, and M. O. Tokhi, “A new hybrid spring brake orthosis for controlling hip and knee flexion in the swing phase,” *IEEE Trans. Neural Syst. Rehabil. Eng. Publ. IEEE Eng. Med. Biol. Soc.*, vol. 9, no. 1, pp. 106–107, Mar. 2001.

[21] W. K. Durfee and A. Rivard, “Design and simulation of a pneumatic, stored-energy, hybrid orthosis for gait restoration,” *J. Biomech. Eng.*, vol. 127, no. 6, pp. 1014–1019, Nov. 2005.

[22] M. Goldfarb and W. K. Durfee, “Design of a controlled-brake orthosis for FES-aided gait,” *IEEE Trans. Rehabil. Eng. Publ. IEEE Eng. Med. Biol. Soc.*, vol. 4, no. 1, pp. 13–24, Mar. 1996.

[23] R. Kobetic, E. B. Marsolais, R. J. Triolo, D. T. Davy, R. Gaudio, and S. Tashman, "Development of a hybrid gait orthosis: a case report," *J. Spinal Cord Med.*, vol. 26, no. 3, pp. 254–258, 2003.

[24] A. Kangude, B. Burgstahler, and W. Durfee, "Engineering evaluation of the energy-storing orthosis FES gait system," *Conf. Proc. Annu. Int. Conf. IEEE Eng. Med. Biol. Soc. IEEE Eng. Med. Biol. Soc. Conf.*, vol. 2010, pp. 5927–5930, 2010.

[25] H. A. Quintero, R. J. Farris, M. Goldfarb, and W. K. Durfee, "Feasibility of a Hybrid-FES System for Gait Restoration in Paraplegics," *Conf. Proc.*, vol. 2010, pp. 483–486, 2010.

[26] W. K. Durfee and A. Rivard, "Preliminary Design and Simulation of a Pneumatic, Stored-Energy, Hybrid Orthosis for Gait Restoration," pp. 235–241, Jan. 2004.

[27] M. Goldfarb, K. Korkowski, B. Harrold, and W. Durfee, "Preliminary evaluation of a controlled-brake orthosis for FES-aided gait," *IEEE Trans. Neural Syst. Rehabil. Eng. Publ. IEEE Eng. Med. Biol. Soc.*, vol. 11, no. 3, pp. 241–248, Sep. 2003.

[28] A. Kangude, B. Burgstahler, J. Kakastys, and W. Durfee, "Single channel hybrid FES gait system using an energy storing orthosis: preliminary design," *Conf. Proc. Annu. Int. Conf. IEEE Eng. Med. Biol. Soc. IEEE Eng. Med. Biol. Soc. Conf.*, vol. 2009, pp. 6798–6801, 2009.

[29] A. J. del-Ama, A. D. Koutsou, J. C. Moreno, A. de-los-Reyes, A. Gil-Agudo, and J. L. Pons, "Review of hybrid exoskeletons to restore gait following spinal cord injury," *J. Rehabil. Res. Dev.*, vol. 49, no. 4, pp. 497–514, 2012.

[30] D. A. Winter, *Biomechanics and Motor Control of Human Movement*. John Wiley & Sons, 2009.

[31] R. Drillis, R. Contini, and M. Bluestein, "Body Segment Parameters; a Survey of Measurement Techniques," *Artif. Limbs*, vol. 25, pp. 44–66, 1964.

[32] S. E. Irby, K. R. Kaufman, R. W. Wirta, and D. H. Sutherland, "Optimization and application of a wrap-spring clutch to a dynamic knee-ankle-foot orthosis," *IEEE Trans. Rehabil. Eng. Publ. IEEE Eng. Med. Biol. Soc.*, vol. 7, no. 2, pp. 130–134, Jun. 1999.

[33] R. C. Juvinall and K. M. Marshek, *Fundamentals of Machine Component Design, 5th Edition*. Wiley Global Education, 2011.

[34] J. Gere and B. Goodno, *Mechanics of Materials*. Cengage Learning, 2012.

Appendix A Previous ESO Art

A.1 First Generation ESO

This project was the initial design of the ESO device [21]. Several energy storage elements and systems were considered and analyzed. Mechanical springs, gas springs, and pneumatic air cylinders were chosen as options to act as energy storage elements for the walking device. The project focused on how to turn these mechanical components into an energy storage system. The efficacy of each of these systems and components will be analyzed individually in later sections. Mechanical springs were decided to be omitted from this initial design, and the initial design of the ESO was a combination of a gas spring and a pneumatic energy transfer system.

Each system has a different function in completing gait. The pneumatic system was used to extend the hip during gait. Two air cylinders are used for each leg to complete the pneumatic system. The air cylinder at the knee joint acts as the storage device that stores energy in the form of compressed air. The energy for this system comes from the user's quadriceps as the knee joint extends compressing air inside the knee cylinder. Compressed air is then transferred to the cylinder located at the hip joint through a hose. The piston then extends causing extension in the hip driving the hip from 10 degrees of flexion to 25 degrees of extension. The gas springs return the hip and knee joint back to the equilibrium position of the gait cycle. Two gas springs were needed for

each leg and one was located at the knee and the other was located at the hip. Together these components used and stored energy to complete the gait cycle.

Analysis of the design of the first generation ESO device included software simulation and bench top testing. Software simulation of the ESO design was completed using ADAMS software. The leg was made from two links with a joint. The two energy storage systems were placed in their respective locations on the links and the simulation was ran to gather results of the modeled design. By running the simulation data could be collected about the velocities, angles of the joints/links, and mounting locations of the design. Other key results of the simulation were stroke lengths and the needed forces of the mechanical components of the design. Bench top testing was used to prove the modeling results. A prototype leg was constructed from wood with similar center of mass properties as an actual leg. Then the mechanical components were placed on the leg and data was collected for comparison with the simulation. From the testing and simulations the required energy from the quadriceps to drive the system was 8.9 J. Quadriceps can realistically provide 14 J. Longevity problems, like muscle fatigue, will be encountered in the quadriceps if more energy is used during the stimulation. The initial ESO design proved that the design is feasible within the capabilities of stimulating the quadriceps.

A.2 Second Generation ESO

The second generation design of the ESO device started investigating new energy storage elements and addressing the design issue of locking the joints during the gait phases [28]. Gas springs were explored again, but were decided to be inadequate for the new design. Instead of the gas springs being used to return the leg to gait equilibrium, a new mechanical energy storage element was used. This new component was elastomer bands, commonly known as rubber bands.

The first generation design did not address the issue of joint locking during the gait and while standing. When the knee and hip extend, the joints need to be locked in place for a brief period of time, especially while the other leg is completing the gait cycle. Also the user should be able to stand upright in the locked device when gait is no longer desired. The new design addressed this problem through the use of a braking system. Wrap spring brakes located at both the knee and hip became the braking system for the new design. Through the use of a solenoid the wrap spring brake could be locked or unlocked at any leg angle. Another consideration for the device braking system in the second generation design was hydraulics, but this system proved to be problematic.

Bench top testing was completed for this new design. The testing investigated each of the mechanical components of the design. Leakage, dead volume, output force and energy storage were analyzed for the pneumatic cylinder system. For the braking system the

holding torque, slip, power intake, solenoid stroke and engagement force were all tested. Testing of the rubber bands included how many rubber bands are needed to achieve the desired output force and displacement.

Clinical testing on one SCI user was completed for the second generation ESO design. The test included one SCI user standing with parallel bars for stability. This ensured that a user could stand in the device and the braking system would prevent collapse. The user's quadriceps was not capable of receiving electrical stimulation so walking tests could not be completed.

A.3 Second Generation ESO Continuation

The continuation of the ESO device design included the optimization of all of the energy storage elements [24]. No new components or systems were changed from the second generation. Instead the study explored component specifications and mounting locations. The goal of the study was to transfer energy as efficiently as possible from the knee to the hip. Adequate posture and maintaining joint range of motion had to be maintained for the optimal design. The study, which was simulated using Matlab, accounted for force/torque, power and energy requirements of the system. Number of needed rubber bands and band mounting locations are one key result of the study. Time to complete one gait cycle was also investigated along with air cylinder stroke length and bore size.

A.4 Previous ESO component notes

Gas springs

The gas springs work by compressing nitrogen gas in a cylinder. The advantage of these springs is their ability to operate at high pressures (50-100 psi). High forces can then be achieved due to the high pressure. The technology that makes the gas springs attractive is the ability of the component to maintain a constant high force. This means the force will not change as the joint angle is changed. Another positive of gas springs are their capability of storing high amounts of energy while remaining small and light. Leakage and loss of pressure are not an issue with gas springs meaning they have long life. Several disadvantages of gas springs have presented themselves in previous designs. Although many different gas springs are readily available, they are difficult to adjust for each different user. The variance in height and weight means a different gas spring may have to be used. An issue with this is the gas springs will be different sizes making it difficult to mount for each case.

Pneumatic energy storage elements

Air cylinders work in a similar way to the gas springs. The difference being instead of using compressed nitrogen gas, air cylinders use compressed air at high pressures to produce a force. Pneumatic components like air cylinders have high energy to weight ratios, even higher than gas springs. Another benefit is that air cylinders come many different sizes and pressures that can be adjusted to a desired output force. The advantage

of pneumatics for the ESO is the ability to transfer energy in the form of compressed air from one location to the other (knee to hip). The pneumatic components needed for the ESO are a hose, a valve, and air cylinders. Energy can then be transferred from the quadriceps to the knee joint and on to the hip joint. Several issues do exist for the pneumatic system. The first is the dead volume in the system from the valves. This results in a significant energy loss. The other problem with pneumatics is their inability to stop the joints. Significant damping is present in the pneumatic components and they act like a spring when the joints need to be locked for stability and energy conservation during gait.

Hydraulic systems

A hydraulic system is also capable of serving as an energy storage system in the ESO design. The potential of hydraulic systems is they can double as both the energy storing system and braking system, unlike pneumatic systems. The reason for this is the hydraulic oil is incompressible and the air in pneumatics is not. This means hydraulic systems can be stopped suddenly and efficiently at any desired joint angle. Disadvantages do exist for the hydraulic ESO systems. Possible leakage of the hydraulic fluid is a significant risk. Also if the fluid has leaked too much and needs to be replaced, this means the device will need periodic maintenance which may not always be possible for the user. Previous analysis also determined that the flow losses across the hydraulic valves are unacceptably high for the energy storage system of the ESO device. Additional

problems are the components are large and heavy causing the overall device to weigh more than the acceptable device weight.

Elastomers (rubber bands)

Elastomers are a different mechanical component then the others previously described. Not only are rubber bands lighter than the traditional energy storage components, they are also smaller in size and profile. The advantage of rubber bands in the ESO design was their ability to store more energy per unit weight than any other component. Also because rubber bands were easy to couple together and take on and off they offer adjustability between user's size and weight that was not possible with other components, which have to be removed and remounted to adjust to the varying size of users. Issues were found using elastomers as the energy storage system in the ESO. The first is that rubber bands lose energy during the extension and retraction process. Since energy is limited in the ESO device and comes from the user's quadriceps, minimal energy loss is important to prevent muscle fatigue. Another issue is that all rubber bands wear out faster than other components. This will lead to inadequate performance towards the end of the rubber bands life when they get stretched out. To resolve this issue the rubber bands will need to be frequently replaced.

Wrap spring brakes (WSB)

Wrap spring brakes were used for the braking system in the ESO design. These components allow rotation in one direction while the wrap spring is locked. As the knee

and hip is extended the wrap spring brake prevents the joint from rotating in the opposite direction. Once full extension was reached the joint was locked in place decreasing the muscle fatigue of holding the knee at extension. If the wrap spring was unlocked the joint could rotate freely in both directions. An additional advantage of the braking system was collapse prevention. As long as the wrap spring was locked the braking system prevented collapse, even if the device experiences a power failure because the wrap spring power off position is locked. Wrap spring brakes have high torque to weight and torque to power ratios.

Appendix B Leg Kinematics

Segment	Definition	Segment Weight/Total Body Weight	Center of Mass/ Segment Length Proximal	Distal	Radius of Gyration/ Segment Length C of G Proximal	Distal	Density
Hand	Wrist axis/knuckle II middle finger	0.006 M	0.506	0.494 P	0.297	0.587	0.577 M	1.16
Forearm	Elbow axis/ulnar styloid	0.016 M	0.430	0.570 P	0.303	0.526	0.647 M	1.13
Upper arm	Glenohumeral axis/elbow axis	0.028 M	0.436	0.564 P	0.322	0.542	0.645 M	1.07
Forearm and hand	Elbow axis/ulnar styloid	0.022 M	0.682	0.318 P	0.468	0.827	0.565 P	1.14
Total arm	Glenohumeral joint/ulnar styloid	0.050 M	0.530	0.470 P	0.368	0.645	0.596 P	1.11
Foot	Lateral malleolus/head metatarsal II	0.0145 M	0.50	0.50 P	0.475	0.690	0.690 P	1.10
Leg	Femoral condyles/medial malleolus	0.0465 M	0.433	0.567 P	0.302	0.528	0.643 M	1.09
Thigh	Greater trochanter/femoral condyles	0.100 M	0.433	0.567 P	0.323	0.540	0.653 M	1.05
Foot and leg	Femoral condyles/medial malleolus	0.061 M	0.606	0.394 P	0.416	0.735	0.572 P	1.09
Total leg	Greater trochanter/medial malleolus	0.161 M	0.447	0.553 P	0.326	0.560	0.650 P	1.06
Head and neck	C7–T1 and 1st rib/ear canal	0.081 M	1.000	— PC	0.495	0.116	— PC	1.11
Shoulder mass	Sternoclavicular joint/glenohumeral axis	—	0.712	0.288	—	—	—	1.04
Thorax	C7–T1/T12–L1 and diaphragm*	0.216 PC	0.82	0.18	—	—	—	0.92
Abdomen	T12–L1/L4–L5*	0.139 LC	0.44	0.56	—	—	—	—
Pelvis	L4–L5/greater trochanter*	0.142 LC	0.105	0.895	—	—	—	—
Thorax and abdomen	C7–T1/L4–L5*	0.355 LC	0.63	0.37	—	—	—	—
Abdomen and pelvis	T12–L1/greater trochanter*	0.281 PC	0.27	0.73	—	—	—	1.01
Trunk	Greater trochanter/glenohumeral joint*	0.497 M	0.50	0.50	—	—	—	1.03
Trunk head neck	Greater trochanter/glenohumeral joint*	0.578 MC	0.66	0.34 P	0.503	0.830	0.607 M	—
Head, arms, and trunk (HAT)	Greater trochanter/glenohumeral joint*	0.678 MC	0.626	0.374 PC	0.496	0.798	0.621 PC	—
HAT	Greater trochanter/mid rib	0.678	1.142	—	0.903	1.456	—	—

*NOTE: These segments are presented relative to the length between the greater trochanter and the glenohumeral joint.

Source Codes: M, Dempster via Miller and Nelson; *Biomechanics of Sport*, Lea and Febiger, Philadelphia, 1973. P, Dempster via Plagenhoef: *Patterns of Human Motion*, Prentice-Hall, Inc. Englewood Cliffs, NJ, 1971. L, Dempster via Plagenhoef from living subjects; *Patterns of Human Motion*, Prentice-Hall, Inc., Englewood Cliffs, NJ, 1971. C, Calculated.

Figure Appendix B.1 Anthropometric data, reprinted from [30]. This is used to define leg kinematics and component characteristics for the ESO design.

Appendix C Wave vs. Coil Springs

Wave springs were a potential replacement to conventional coil springs for the ESO. Wave spring manufacturers boast that the wave design reduces the vertical space needed in applications by up to 50%. This is the case because the compressed height of wave springs is less than the compressed height of coil springs for the same load and displacement. Wave springs are available in a wide variety of sizes and spring rates which meet the spring requirements of the ESO. Using the spring requirements for the equilibrium springs of the ESO device a coil spring and wave spring were chosen and compared. The wave spring had a larger diameter than the coil spring. Wave springs had to be stacked for required spring displacement and rate, so they are not much shorter than coil springs. This is due to the needed stroke length of the spring to move the hip and knee joints to the proper angles. For the ESO application the vertical space will not be reduced by 50%, but more like 20% by wave springs. More vertical space is available, parallel to the thigh, than radial space, and the wave spring was 0.3 inches larger in diameter than the coil spring. The major factor in the design was the weight of the device. The wave spring websites claim that the wave springs reduce the weight of the component by up to 50%. No information could be found to support this, as the weights of the springs are not provided. Analysis was completed to determine if the wave springs

weigh less, but still have the same force output. This was completed by calculating the energy density of wave and coil springs for different spring rates (Figure Appendix C.1).

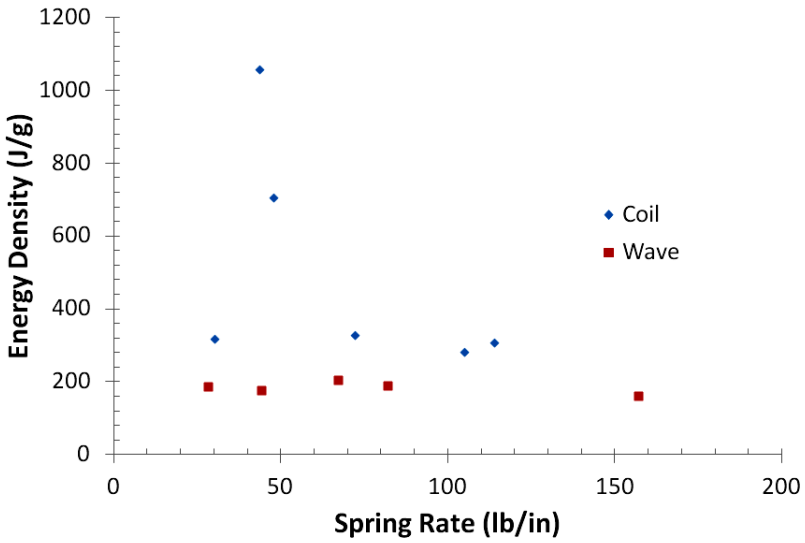

Figure Appendix C.1 - Spring energy density as a function of spring rate

Findings show that wave springs do not actually have a higher energy density than coil springs. Even some of the coil springs with similar spring rates have significantly higher energy densities. This indicates that coil springs would be a better option than wave springs for the energy storage components.

Appendix D Wrap Spring Brakes

D.1 Wrap Spring Unlocking Data

This section determines and measures the tension force needed to unlock the wrap spring used in the ESO device. This data will show the required displacement and tension force needed to unlock the control tang. Using this data a mechanical locking/unlocking device can be designed.

The equipment needed for testing was a force gage, ruler, and wrap spring. Wagner Instruments Force Five handheld digital force gage was used as the force gage. The wrap spring tested is the wrap spring used in the ESO device.

Measurements for the wrap spring control tang tension force were taken by starting the wrap spring in locked position. Then the wrap spring control tang was actuated at 0.5 cm intervals using the ruler and the tension force recorded by the force gage until the control tang was actuated 2.5 cm. Three trials were performed.

To measure the displacement to unlock the wrap spring the control tang was displaced in millimeter increments. At each increment a force was applied to the leg segment seeing if the joint had unlocked. The displacement causing the joint to unlock was then recorded in millimeters. This was repeated for three trials.

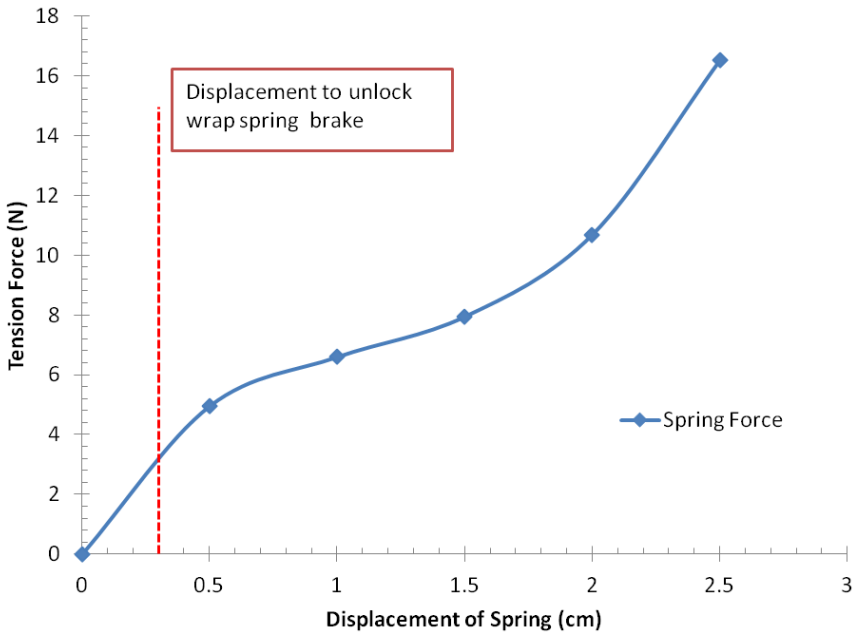

Figure Appendix D.1 - Wrap spring unlocking data. The solid line is the tension force needed to displace the wrap spring control tang. The dotted line represents the displacement needed to completely unlock the wrap spring.

Figure Appendix D.1 shows the data collected for the wrap spring control tang unlocking. As the control tang on the wrap spring was pulled the tension force increases relatively linearly. The control tang was displaced to a value of 2.5 cm. The maximum tension force that was measured was 16.5 N.

The other set of data that was collected was the displacement needed to unlock the wrap spring. The dotted line (Figure Appendix D.1) represents the needed displacement of the wrap spring control tang to unlock the joints. 3 millimeters was the displacement needed to unlock the wrap spring. The resulting force was 3.3 N.

Based on the data collected a displacement distance to unlock the wrap spring control tang was defined. To ensure that the tang will be completely unlocked every time in the actual device the displacement of the tang was increased. This will add an additional safety factor to the make sure the wrap spring is unlocked during operation. A displacement of 0.5 cm will suffice for this wrap spring application. The resulting force was 4.9 N.

Knowing the values of the displacement and tension force of the study, a mechanical actuation mechanism was designed. The goal of the mechanism was to toggle the wrap spring between the locked and unlocked positions, while using the least amount of energy as possible. If possible the unlocking energy source should be shut off to conserve energy in the unlocked position, since the wrap spring is required to stay in this position for some time. Possible control tang actuation devices could be solenoids, linkages, or motors.

D.2 Servo Motor Analysis

The section uses data about the unlocking of the ESO wrap spring to select a servo motor to lock and unlock the wrap spring brake. The study explores the servo motor angle of travel, the motor arm length, the servo motor torque and the actuation time to unlock the wrap spring. By exploring this information a suitable servo motor was selected for the ESO joint locking/unlocking device.

The analysis of the servo motor was completed using Matlab software. A servo motor can be actuated to a maximum angle of 180 degrees. The program used equations over the motor angle of travel and plotted the data of interest for a specific displacement of the wrap spring unlocking control tang. For this analysis the tang displacement was set to 0.5 cm. From this data a proper servo motor was selected, and the motor arm length and angle of travel were specified.

First the displacement of the control tang was defined in the program. After this a range of the motor angle of travel was set; in this case ranging from 20 degrees of travel to 180 degrees. Then the motor arm length was defined over the range of travel and plotted. Next the motor torque to unlock the wrap spring for each case was found using previous unlocking force data. These torque results were also plotted against the different angles of travel. Then a servo motor was selected that met the torque requirements. Last the actuation time was calculated based on the motor specifications. For this analysis the Hitec HS-35HD nano servo motor was selected because of its small size and weight.

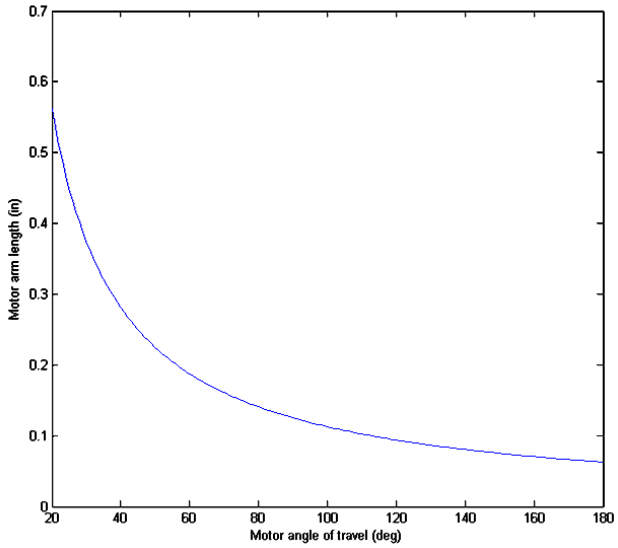

Figure Appendix D.2 - Motor arm length vs. motor angle of travel

Figure Appendix D.2 shows the data collected for the servo motor arm length. As the motor angle of travel goes from 100 degrees to 180 degrees the length does not change significantly, and was around 0.1 in. The length decreases exponentially before this range and the maximum motor arm was 0.55 in. at 20 degrees of travel.

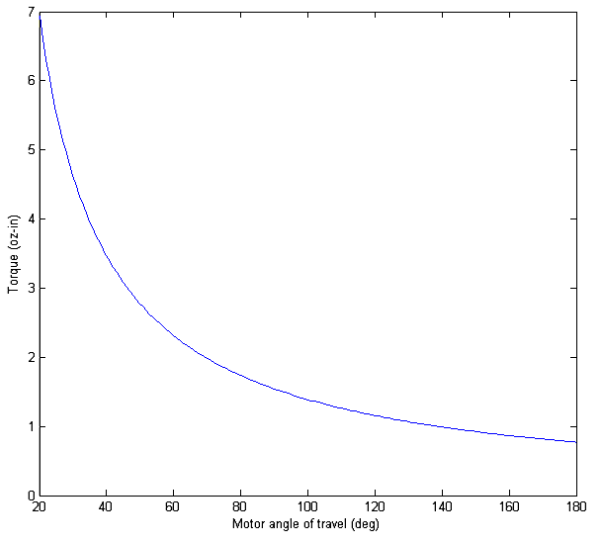

Figure Appendix D.3 - Needed motor torque vs. motor angle of travel

Figure Appendix D.3 shows the data collected for the needed servo motor torque. As the angle of travel goes from 100 degrees to 180 degrees the torque does not change significantly. The torque was approximately 1 oz-in. Before this the torque decreases drastically as the angle of travel was increased. The max torque occurred at 20 degrees of travel and had a value of 7 oz-in.

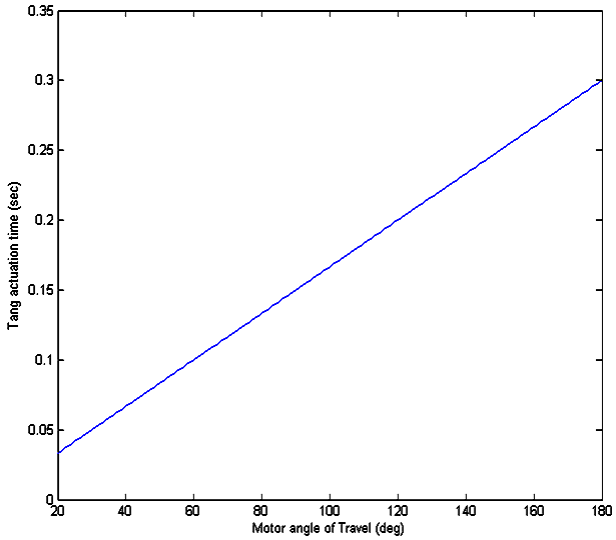

Figure Appendix D.4 - Control tang actuation vs. motor angle of travel

Figure Appendix D.4 shows the data collected for the actuation time of the servo motor selected. As the angle of travel was increased for the servo motor the actuation time increased linearly. The least amount of actuation time occurred at 20 degrees of travel, and it was 0.04 seconds. The maximum actuation time, which is not desired, occurred at 180 degrees of travel with a value of 0.3 seconds.

Based on the data collected a suitable servo motor was selected for the ESO application and the variable of interest, the actuation time, was found. When picking a servo motor the important factor is whether the motor can meet the desired torque for any of the angles of travel.

For the ESO application a realistic servo motor angle of travel to achieve the fastest actuation time was around 60 degrees. Also the angle of travel does not want to be so small that the arm length is significant and impacts the packaging and size of the joint wrap spring brake system. Defining this angle of travel the actuation time was 0.1 seconds. The torque at this location was 2.2 oz-in, and the motor arm length was 0.2 in. This means that the Hitec servo motor will suffice for the ESO application.

Appendix E Bill of Materials

Table Appendix E.1 is the bill of materials of the ESO prototype used for bench-top testing.

Table Appendix E.1 - ESO prototype bill of materials

No.	Purchasing Company	Description	Size	Quantity	Cost	Total
1	Online Metals	Aluminum 6061-T6 Bare Drawn Tube	0.375"x 0.049"x 0.277", 60" Length	1	$15.75	$15.75
2	Online Metals	Aluminum 6061-T6511 Bare Extruded Round	0.5", 36" Length	1	$2.97	$18.72
3	Online Metals	Aluminum 6061-T6511 Bare Extruded Rectangle	0.5"x 2", 36" Length	1	$15.87	$34.59
4	McMaster-Carr	Sure-Grip Cushioned Loop Clamp, Aluminum	0.375" Dia. Pack of 5	1	$5.53	$40.12
5	McMaster-Carr	Two-Piece Clamp-on Shaft Collar, Aluminum	0.375" Dia.	10	$48.50	$88.62
6	McMaster-Carr	Highly Corrosion-Resistant 6063 Aluminum Square Tube	0.125"x 0.75"x 0.75", 36" Length	1	$7.89	$96.51
7	McMaster-Carr	White Delrin Rod	2" Dia., 12" Length	1	$16.69	$113.20
8	McMaster-Carr	Plastic Dowel Pin	0.25" Dia., 0.75" Length Pack of 50	1	$3.37	$116.57
9	McMaster-Carr	Alloy Steel Dowel Pin	0.25" Dia., 0.75" Length Pack of 25	1	$5.24	$121.81
10	Amazon	Velcro Velstretch Strap	1x27 in 2-pack black	4	$22.96	$144.77
11	McMaster-Carr	Constant-Force Springs		3	$55.74	$200.51
12	McMaster-Carr	PTFE/Oil-Lubricated SAE 841 Bronze Flanged Sleeve Bearings		10	$15.20	$215.71
13	McMaster-Carr	Alloy Steel Socket Head Cap Screws		1	$7.58	$223.29
14	McMaster-Carr	Alloy Steel Flat-Head Socket Cap Screws		1	$8.29	$231.58
15	SDP/SI	Aluminum Alloy Gear	24 D.P., 45 Teeth, 20° Pressure Angle, AGMA Q10 Quality	2	$61.72	$293.30

Appendix F SimMechanics

F.1 SimMechanics Overview

SimMechanics was the tool used to perform dynamic simulations for the ESO concept. SimMechanics is a Matlab Simulink software package with capabilities of constructing mechanical systems and performing analysis. For this project three separate models were created in SimMechanics. These three models were intended to simulate ESO phases of gait.

F.2 Models

The first model was for the knee extension simulation. This SimMechanics block diagram is in Figure Appendix F.1. The solid models (linkages) of the simulation are the bigger boxes with connections for components labeled *pivot_mount, thigh_link* and *foot_link*. For these linkages dimensions and weights based on the center of gravity of the legs were specified. The hip and knee joints were modeled as revolute joints labeled *Revolute Joint* and *Revolute Joint1*. Within these joints an initial starting position of the joints was defined for the simulation. Also the allowable joint actuation angles were specified in the block diagram *Rotational Hard Stop*. During the simulation the parameter of interest was the joint angle with respect to time. To collect this data a scope block was set-up at both the hip and the knee joints. The spring forces in the simulations were represented as internal force members. They are labeled as *TSpring* and *KESpring*. A

constant spring force of 107 N was input into the internal force blocks for the constant force spring force. For the knee extension simulation an external force was introduced into the system by a block called a *Signal Builder*, and this simulates the quadriceps torque entering the system.

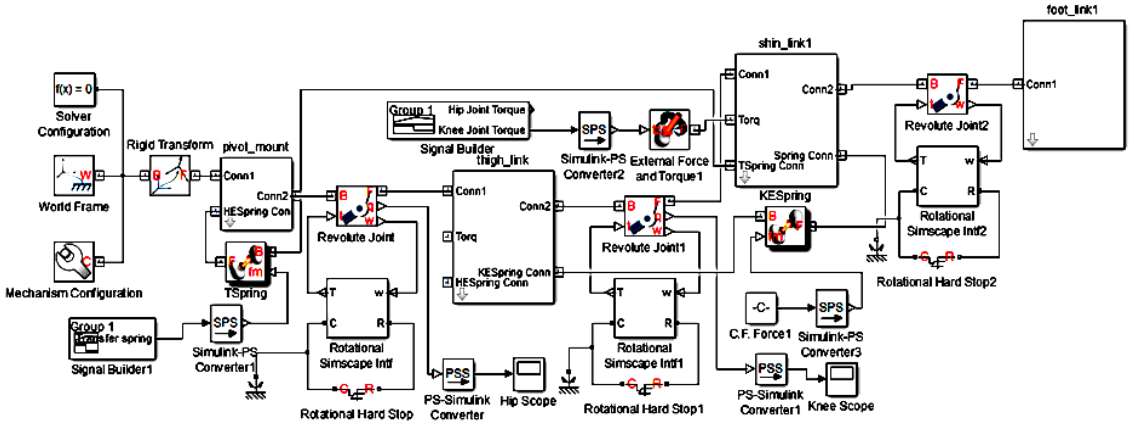

Figure Appendix F.1 - Simulation block diagram for knee extension

The next simulation block diagram is shown in Figure Appendix F.2. This was the block diagram for the hip extension simulation. In this simulation the lengths and mass of the linkages were altered to match the parameters of the whole leg and HAT segments. The joint starting positions and actuation limits were also changed to match hip extension characteristics. Two scopes were used for this simulation so the angle position as a function of time was found for both joints.

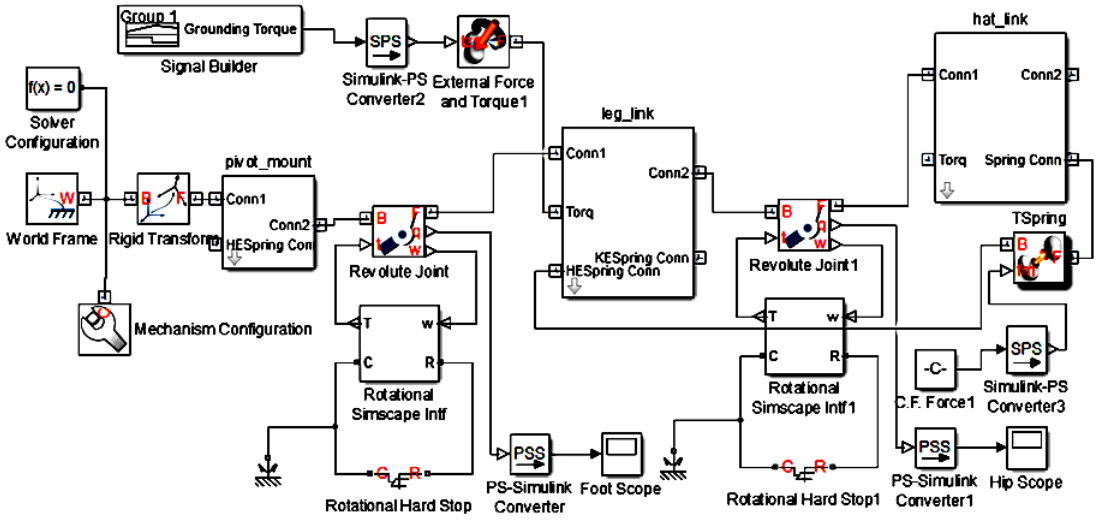

Figure Appendix F.2 - Simulation block diagram for hip extension

The third simulation block diagram is shown in Figure Appendix F.3 and was for the return to equilibrium position simulation. Solid body members for this simulation include the thigh segment, shin segment and the foot. Data was collected for the joint angles of the hip and knee as a function of time. The hip equilibrium and knee equilibrium spring force was implemented into the simulation to return the simulation linkages back to the equilibrium position. Simulation videos can be seen in the simulation viewer in Matlab to clarify if the simulation video was acting as expected.

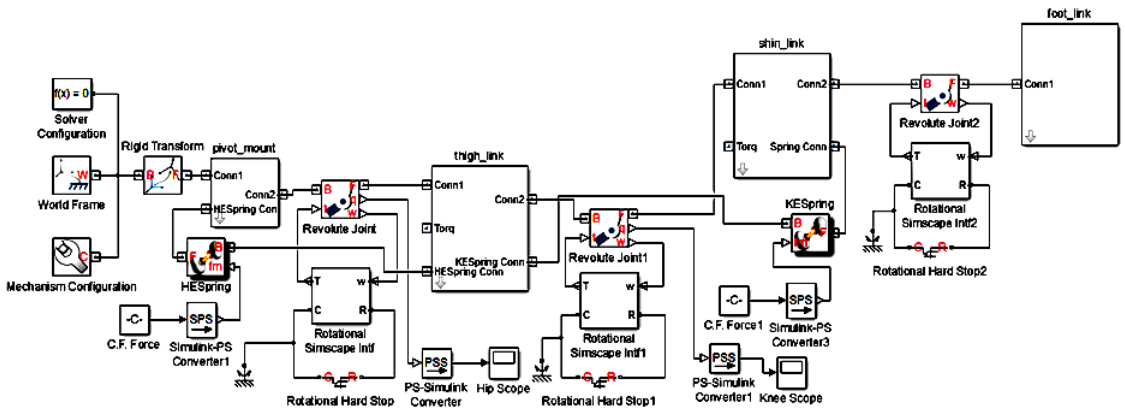

Figure Appendix F.3 - Simulation block diagram for hip and knee return to equilibrium

F.3 Additional Information and Documentation

Additional information about SimMechanics can be found on the Mathworks website (http://www.mathworks.com/). On this website tutorials and web chat chains were found to gain a better understanding of the many capabilities of SimMechanics.

F.4 Tutorials

Several tutorials were helpful in the completion of the ESO simulations.

1. http://www.mathworks.com/help/physmod/sm/mech/gs/what-you-can-do-with-simmechanics-software.html
2. http://www.mathworks.com/help/physmod/sm/ref/externalforceandtorque.html
3. http://www.mathworks.com/help/physmod/sm/ref/internalforce.html
4. http://www.mathworks.com/help/physmod/sm/ug/sense-double-pendulum-motion.html
5. http://www.mathworks.com/help/physmod/sm/ug/model-double-pendulum.html

6. http://www.mathworks.com/help/physmod/sm/ug/model-binary-link.html

7. http://www.mathworks.com/help/physmod/sm/ug/model-pivot-mount.html

8. http://www.mathworks.com/help/physmod/sm/ug/represent-binary-link-frame-tree.html

Appendix G Motion Capture System

The motion capture system used to test the prototype of the ESO had three main components that are explained. Figure Appendix G.1 was the first component needed for the motion capture system and it is the camera. The camera that was used is the Basler Scout camera. This camera was mounted on a tripod with the proper field of view to prevent prototype distortion in the video. An Ethernet cord connected the camera to the computer where video recording software captured testing video.

Figure Appendix G.1 - Basler Scout camera, reprinted from http://www.baslerweb.com/

The next component was the video recording software. This software is called Pylon Viewer and has many recording capabilities. The software interface is in Figure Appendix G.2. The first step was to recognize the camera by the computer. This involved steps that would be similar to selecting an Ethernet internet and entering the I.P. address. Once the camera was selected the field of view was shown by clicking the continuous

button on the top interface bar. This helped align the prototype in the camera field of view for testing. To start recording video the red record button was clicked. Another screen popped up where video recording parameters were set. Parameters included the number of frames per second and the video recording time. After record was pressed the prototype testing was started. When the video time had concluded the software stopped the recording on its own and automatically saved the video as an .avi file. The file was viewed to see if the testing looked as intended. Multiple videos can be taken for multiple tests and the program will keep saving new files. Pylon Viewer software information was found at http://www.baslerweb.com/feedback/pylon-Stoerer-106621.html.

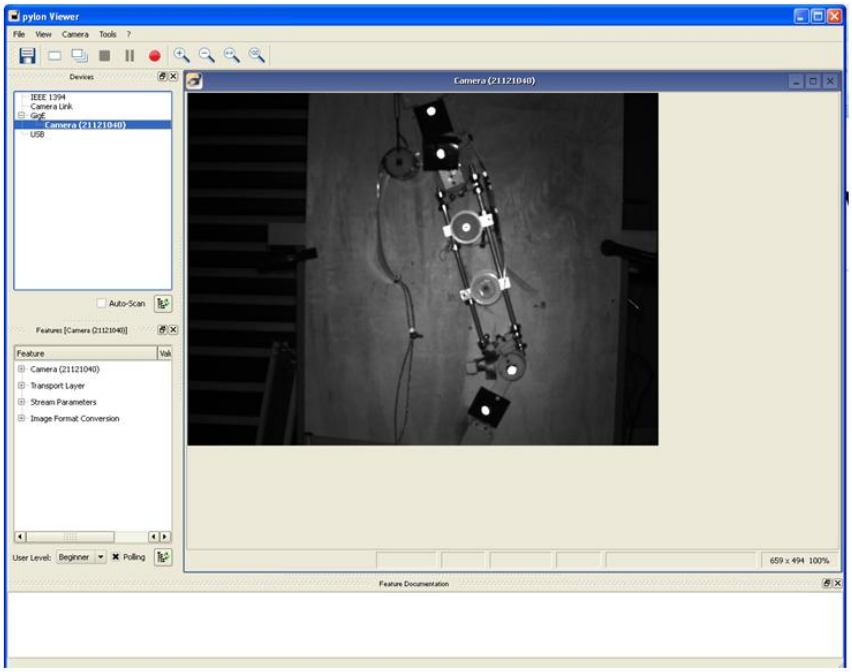

Figure Appendix G.2 - Pylon viewer software interface

After the video files were created they were opened in software for motion analysis. This software was MaxTRAQ (Innovision). Free trials of this software were found at http://www.innovision-systems.com/home.html. The interface of the software is shown in Figure Appendix G.3. The video files of interest were opened and analyzed in MaxTRAQ. The software works by recognizing retro reflective points of interest on the prototype. The points were defined in the right column by clicking digitize and clicking through where the points are located. Then auto track was selected and when the video is played the software will track the retro reflective points. Sometimes the software lost a point and stopped, and the point had to be selected manually. After the points had been defined in the entire video, analysis was completed. The interest of this dynamic analysis was the prototype joint angles as a function of time. An angle between points was defined in the software. Three points were selected to define an angle, for this case the hip and knee joints. This data was saved to an ASCII file and imported into excel, where the data was plotted as a function of time. A helpful tutorial video for MaxTRAQ was found at http://www.innovision-systems.com/Tours/MaxTRAQ_MaxMATE/MaxTRAQ_MaxMATE.htm.

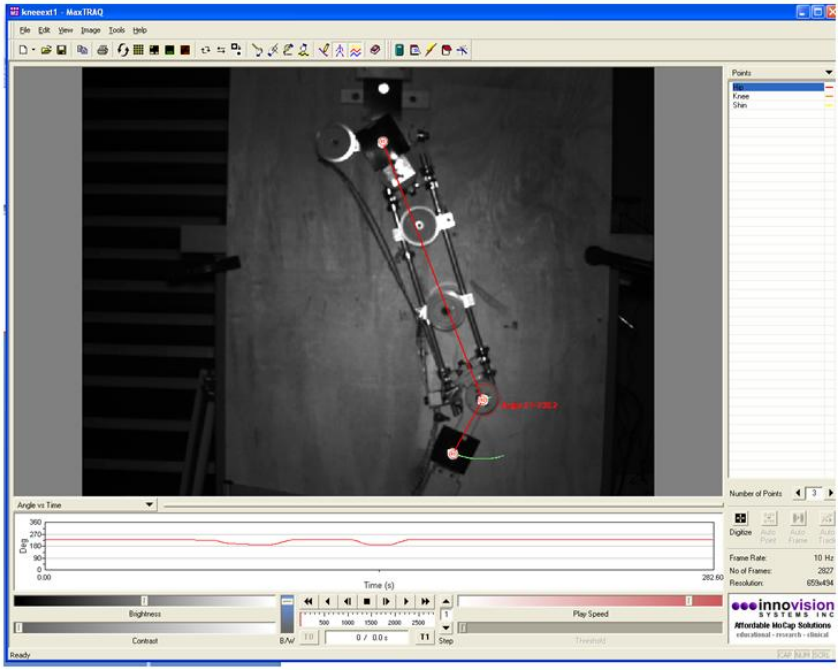

Figure Appendix G.3 - MaxTRAQ software interface

Appendix H ESO Prototype Weight Reduction

The mass of the preliminary thigh prototype was 2.33 kg. Although this was below the requirement for the ESO, weight can be reduced in two areas. The first is with the gears used in the hip joint wrap spring brake. These gears only actuate between the hip joint angles of -10 to 25 degrees, so all the other gear teeth will never mesh. Therefore this part of the gear can be removed while still allowing material for mounting on the shaft. Also additional weight can be removed by drilling holes in the remaining part of the gear as long as enough material is left for the needed part strength.

The second area where weight can be reduced in the ESO is in the constant force springs. The constant force springs have an available stroke length of 52 in. For the ESO an average stroke length of 4 in. is needed for the three springs. Since these are made from stainless steel, significant weight can be reduced by removing the unneeded stroke length of the constant force springs.